https://doi.org/10.5194/egusphere-2024-163
Preprint. Discussion started: 23 January 2024

Cosmogenic ^{3}He chronology of postglacial lava flows at Mt. Ruapehu, New Zealand

Pedro Doll[1], Shaun Robert Eaves[2,3], Ben Matthew Kennedy[1], Pierre-Henri Blard[4], Alexander Robert Lee Nichols[1], Graham Sloan Leonard[5], Dougal Bruce Townsend[5], Jim William Cole[1], Chris Edward Conway[6], Sacha Baldwin[1,*], Gabriel Fénisse[4,*], Laurent Zimmermann[4,*], and Bouchaïb Tibari[4,*]

[1]School of Earth and Environment, University of Canterbury, 20 Kirkwood ave, 8041 Christchurch, New Zealand
[2]Antarctic Research Centre, Victoria University of Wellington, PO Box 600, Wellington 6140, New Zealand
[3]School of Geography, Environment and Earth Sciences, Victoria University of Wellington, PO Box 600, Wellington 6140, New Zealand
[4]CRPG-CNRS, Université de Lorraine, 15 Rue Notre Dame des Pauvres, Vandoeuvre-les Nancy 54000, France
[5]GNS Science, 1 Fairway Drive, Avalon, Lower Hutt 5011, New Zealand
[6]Geological Survey of Japan, National Institute of Advanced Industrial Science and Technology (AIST), 1-1-1 Higashi, Tsukuba, Ibaraki 305-8567, Japan
[*]These authors contributed equally to this work.

Correspondence: Pedro Doll (pedro.doll@pg.canterbury.ac.nz)

Abstract. Accurate volcanic hazard assessments rely on a detailed understanding of the timing of past eruptions. While radiometric methods like ^{40}Ar/^{39}Ar or K/Ar are by far the most conventional lava flow dating tools, their low resolution for young (<20 ka) deposits interferes with the development of precise recent effusive chronologies on most volcanoes. Mt. Ruapehu (New Zealand) has produced many lava flows throughout its history, but the precise timing of many recent eruptions remains largely unknown. In this study, we use cosmogenic ^{3}He exposure dating to provide 23 eruption ages of young lava flows at Ruapehu. We then compare our results with existing ^{40}Ar/^{39}Ar and palaeomagnetic constraints, highlighting the value of cosmogenic nuclides exposure dating in refining recent eruptive chronologies. Of the 23 sampled flows, 16 provided robust eruption ages (5–20% internal 2σ; n$\geq$3) between *ca* 20 and 8 ka, except for one lava erupted at around 43 ka, and their age distribution indicates that, during the last 20 thousand years, effusive activity at Ruapehu peaked at 17–12 ka and at 9–7.5 ka. Nearly identical eruption ages of lavas located in different flanks of the volcanic edifice suggest concurrent activity from multiple vents during relatively short time intervals (0–2 kyr) at around 13, 10 and 8 ka. We analysed four lavas previously dated by ^{40}Ar/^{39}Ar, two of which yielded eruption ages older than the older limit of the 2σ interval of the radiometric dates, but the good clustering of individual samples from our sites suggests that our results better represent these lava flows' real eruption ages. Our ^{3}He-based dates show excellent agreement with palaeomagnetic constraints, suggesting that production rate uncertainties are unlikely to impact the accuracy of our eruption ages. This study demonstrates how cosmogenic nuclides dating can provide greater detail on the recent effusive chronology of statovolcanoes, helping to resolve the low resolution and difficulty in applying radiometric dating methods to young lava flows.

https://doi.org/10.5194/egusphere-2024-163
Preprint. Discussion started: 23 January 2024

1 Introduction

Effusive volcanism is the main mechanism driving edifice growth on stratovolcanoes and poses a great hazard to infrastructure, the natural environment, and local communities' social fabric and livelihoods (Trusdell, 1995; Wilson et al., 2014; Harris, 2015; Jenkins et al., 2017; Tsang and Lindsay, 2020). Accurate hazard assessments rely on precise knowledge of recent eruption footprints, magnitudes and frequencies, and hence accurate dating of eruptive events.

Most chronological studies of lava flows on stratovolcanoes are based on radiometric methods, such as $^{40}Ar/^{39}Ar$ and K/Ar. Recent advances in these methods (Coble et al., 2011; Fleck et al., 2014; Clay et al., 2015) have improved the precision of age determinations for Pleistocene lavas. However, errors on ages of young (<20 ka) products are still too large to precisely resolve recent eruptive chronologies (e.g. Wijbrans et al., 2011; Conway et al., 2016; Ramos et al., 2016; Calvert et al., 2018; Preece et al., 2018; Pure et al., 2020), hindering our ability to discriminate distinct eruptive episodes or to determine temporal relationships between effusive eruptions and other volcanic processes. Alternative methods such as palaeomagnetism or cosmogenic nuclides exposure dating can support radiometric studies, considerably reducing their uncertainties for late Pleistocene and Holocene products (Sherrod et al., 2006; Parmelee et al., 2015; Wright et al., 2015; Greve et al., 2016), and are therefore important to generating more accurate volcanic eruptive histories.

Cosmogenic nuclides are isotopes that originate when primary and secondary cosmic rays interact with atomic nuclei (Leya et al., 2000; Dunai, 2010). Some of them (terrestrial *in-situ* cosmogenic nuclides, or TCNs) are formed in the upper few metres of the Earth's surface and can be used to calculate exposure ages of geological deposits provided they are: rare in geological materials; produced and retained in common minerals; able to be analysed with reasonable confidence; stable or have a half-life comparable to the timescales of the studied process; and have a well-understood origin and the relative contributions of its production mechanisms are known (Dunai, 2010). The number of TCNs that fulfil these requirements and have well-established methodologies developed for Earth science applications is relatively small, and TCNs' production rates and retention efficiency vary across different minerals. ^{3}He is a stable isotope with the highest production rate of all TCNs and a low detection limit in several geological settings (Blard, 2021), which makes it the ideal nuclide for dating young lava flows (Gosse et al., 2001). This gas suffers diffusion loss in felsic minerals (e.g. quartz and feldspars) and in volcanic groundmass at Earth's surface temperatures, and is therefore not normally used for silicic lithologies which are better studied using ^{10}Be or ^{36}Cl. ^{3}He is more efficiently retained in diamonds (inapplicable for exposure dating due to its scarcity), olivines and pyroxenes (Kurz, 1986; Gosse et al., 2001; Shuster et al., 2004; Blard, 2021), so it is suitable for dating basic and intermediate igneous rocks that contain these minerals.

Surface exposure dating using TCNs is applicable to geological deposits that have been brought to the surface and remained exposed to the cosmic ray flux ever since, provided there is no significant erosion or shielding (glacial, snow, debris, soil, tephra, or vegetation cover) which could have affected their cosmogenic nuclide inventory. For young lava flows, $^{3}He_{cos}$ has the potential to resolve events down to 100 years under the most favourable conditions (low magmatic He and eruption ages $\leq$10 ka; Niedermann, 2002) and commonly yields ages with uncertainties of 15–20% (2σ including production rate errors), significantly more precise than traditional radiometric techniques for lavas <20 ka (e.g. Wijbrans et al., 2011; Calvert et al., 2018; Pure et al.,

https://doi.org/10.5194/egusphere-2024-163
Preprint. Discussion started: 23 January 2024

2020). Thus, $^{3}He_{cos}$ can be used to complement chronological studies by providing greater detail on volcanoes' recent edifice construction histories (e.g. Kurz et al., 1990; Foeken et al., 2009; Espanon et al., 2014; Parmelee et al., 2015; Alcalá-Reygosa et al., 2018).

In this paper, we use surface exposure dating with terrestrial *in-situ* cosmogenic ^{3}He ($^{3}He_{cos}$) in pyroxenes and olivines to provide 23 eruption ages of mainly postglacial (<20 ka) lava flows at Mt. Ruapehu, a large (summit 2797 m asl) andesitic stratovolcano located in the centre of North Island, New Zealand. We then compare our results with previous $^{40}Ar/^{39}Ar$ and palaeomagnetically-refined ages, as well as with eruption age assumptions based on geochemical fingerprinting, and test the applicability of $^{3}He_{cos}$ as a lava flow dating tool for stratovolcanoes, showcasing the method's capacity to provide high resolution ages for young lava flows and to identify distinct eruptive episodes in short time intervals.

2 Geological background

2.1 Study area

Ruapehu is a cultural and spiritually significant *Maunga* (Māori word for mountain) for local Iwi (Māori tribes) Ngāti Rangi, Ngāti Tūwharetoa and Uenuku. This volcano is the southernmost continental expression of the Taupō Volcanic Zone (TVZ, Figure 1), related to the Hikurangi Trench, the southern end of the Tonga-Kermadec arc subduction system (Cole and Lewis, 1981). The TVZ can be divided into three segments: the northern, central and southern TVZ (Figure 1a), distinguished by composition and eruptive styles. The northern TVZ is formed by andesitic stratovolcanoes, including Whakaari-White Island and Motuhara off the northeastern coast of North island. The central TVZ is one of the most productive silicic volcanic systems in the world, which has experienced at least 34 caldera-forming events in the last 1.6 Ma, including Taupō and Ōkataina (Houghton et al., 1995; Wilson et al., 2009). The southern zone is dominated by the andesitic stratovolcanoes Ruapehu and Tongariro, with subordinate basalts (e.g. Ohakune Formation basalt).

Ruapehu is the largest and one of the most active stratovolcanoes in mainland New Zealand (Leonard et al., 2021). The current edifice is mostly formed by pyroxene-bearing basaltic andesite, andesite, and dacite lavas, which have been erupted throughout four main constructive periods, and are encompassed in distinct units; Te Herenga (200–150 ka), Waihianoa (150–80 ka), Mangawhero (50–15 ka) and Whakapapa (15–2 ka) formations (Hackett, 1985; Townsend et al., 2017). Contemporary to lava flow emplacement, Ruapehu generated many explosive eruptions (Topping and Kohn, 1973; Donoghue et al., 1995; Pardo et al., 2012), including several plinian events (Pardo, 2012) preserved as tephra sequences on the eastern volcanic ring plain. In this study, we focus on the Whakapapa Formation and the youngest member of the Mangawhero Formation (Figure 1; Table 1), providing greater detail on the recent effusive activity of Ruapehu.

Eruption ages of Ruapehu's lava flows were first determined using K/Ar (Stipp, 1968; Tanaka et al., 1997) and later improved with $^{40}Ar/^{39}Ar$ by Gamble et al. (2003) and Conway et al. (2016). Combining these $^{40}Ar/^{39}Ar$ ages with an extensive geochemical survey, Conway et al. (2016) divided lavas from the Mangawhero and Whakapapa formations into distinctive packages, later formalized as members by Townsend et al. (2017, Table 1). However, many lava flows are only assumed to

https://doi.org/10.5194/egusphere-2024-163
Preprint. Discussion started: 23 January 2024

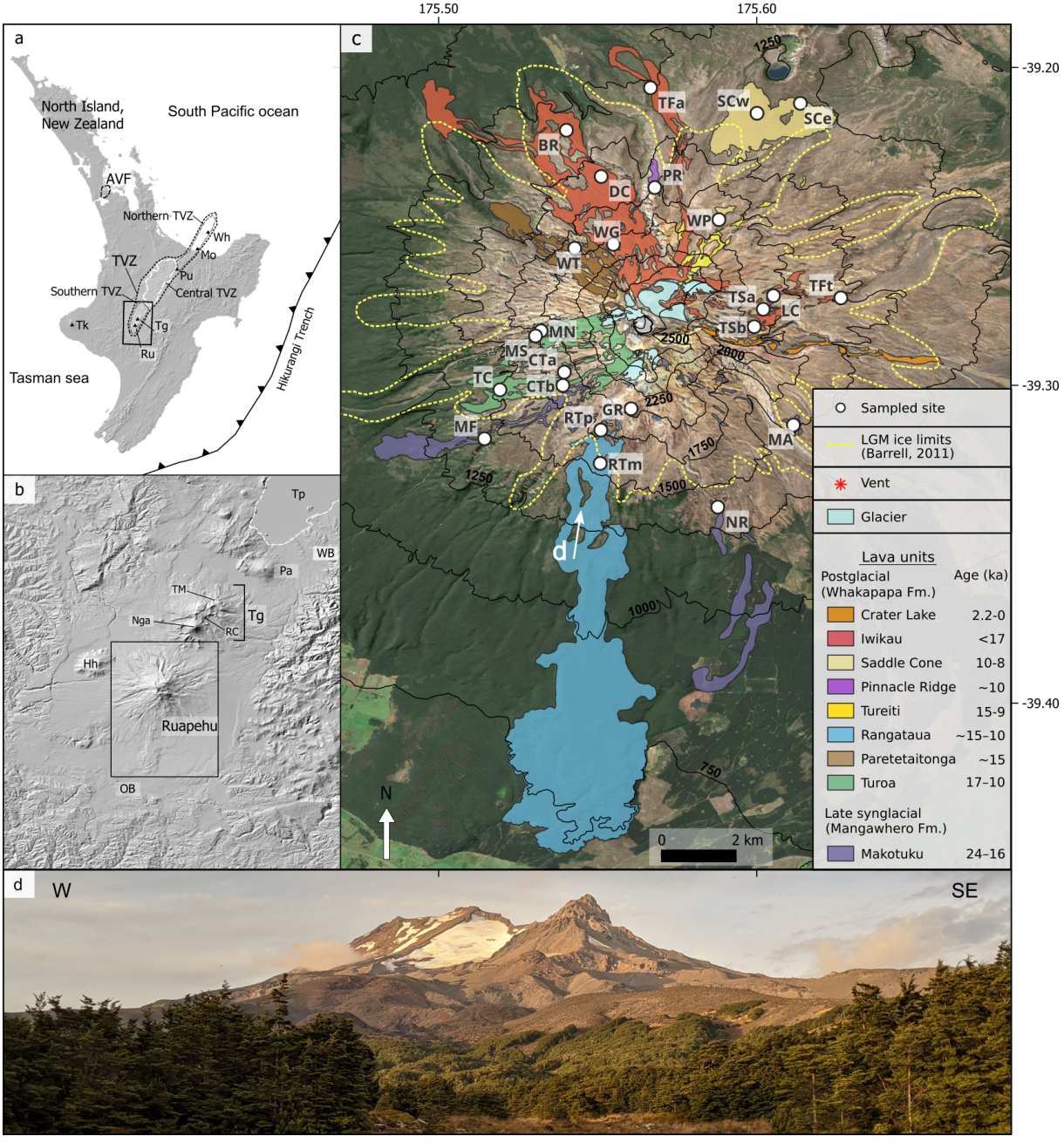

Figure 1. Location map of study area. a) North Island of New Zealand with its main active volcanic areas detailed. (AVF) monogenetic Auckland Volcanic Field; (Wh) Whakaari-White Island; (Mo) Motuhara; (Pu) Putauaki; (TVZ) Taupō Volcanic Zone; (Tg) Tongariro; (Ru) Ruapehu; (Tk) Taranaki. b) Detail of the "Central Plateau", at the southern end of the TVZ. (Tp) Taupō; (WB) Waimarino Basalt; Pihanga (Pa); (Tg) Tongariro; (TM) Te Maari; (Nga) Ngauruhoe; (RC) Red Crater; (Hh) Hauhungutahi; (OB) Ohakune Formation basalt. c) Study area, with Ruapehu's postglacial and late synglacial lava units mapped after Townsend et al. (2017) and sampled sites in this study. Maximum glacial extent during the LGM (last glacial maximum, ~20–15 ka) after Barrell (2011) outlined with black dashed line. (NV) Northern vent; (SV) Southern Vent. Abbreviations next to sampled sites refer to lava flow names, full list in Table A1. d) Photo of Ruapehu taken from the south, with Mangaehuehu Glacier directly beneath Ruapehu's summit (see in subfigure c the viewpoint's location).

https://doi.org/10.5194/egusphere-2024-163
Preprint. Discussion started: 23 January 2024

have been erupted in specific time periods due to their geochemical similarity and/or geographical proximity to flows with geochronological constraints.

Throughout its history, Ruapehu has periodically been extensively covered by glaciers controlling lava flow emplacement (Conway et al., 2015). The edifice displays characteristic erosional and depositional glacial landforms extending from current glaciers down to ∼1200 m asl (Mc Arthur and Shepherd, 1990; Eaves et al., 2016a; Townsend et al., 2017) and conspicuous large and fine-scale features indicative of lava-ice interaction. During heavily glaciated periods, lava emplacement and preservation were restricted to inter-valley ridges, and cooling against ice generated overthickened lava margins (ice-bounded flows; Conway et al., 2015) still visible in the landscape. Based on the distribution of these ice-bounded lava flows, Conway et al. (2016) suggested a peak in glacial expansion between 42 and 31 ka and a reduction in ice thickness between 31 ka and the last stages of the last glacial maximum (LGM) at 20–15 ka (Barrell et al., 2013), prior to the glacial retreat. Effusive deposits erupted after the LGM (postglacial lavas of the Whakapapa Formation, Figure 1) were free to flow to the valley floors and finished shaping the modern landscape observed at Ruapehu. Eaves et al. (2019) provided $^{3}He_{cos}$ ages for moraine groups on the Mangaehuehu valley (south Ruapehu) recording pulsatory glacial retreat after the LGM. Based on $^{3}He_{cos}$ exposure ages of boulders, they proposed moraine construction periods and associated equilibrium line altitudes of 2100 m asl at ∼14–11 ka, 2250 m asl at 4.5 ka, and 2300 m asl at 200–500 yr ago. Present glaciers on Ruapehu (3.0 km^2 on 2016; Eaves and Brook, 2021) are restricted to some upper catchment areas over 2250 m asl, the largest of which is located on its summit plateau at >2500 m asl.

2.2 Previous chronological studies on postglacial lavas

The first constraints on eruption ages of Whakapapa lavas were given from studies of tephra layers (Topping, 1974; Price et al., 2012). Conway et al. (2016) were the first to provide absolute ages using $^{40}Ar/^{39}Ar$, for which samples from slowly-cooled lava interiors are needed, as Ar analyses are done in crystalline groundmass (glass contents <5%) with large microlites. The lack of abundant exposures of lava interiors limited its application to only 10 flows, and although this technique yielded reasonably precise ages for lavas >20 ka, their relative errors increase with decreasing age, varying between 16 and 23% for 20–11 ka deposits and 32 and 1000% for Holocene lavas (see Table 1).

Greve et al. (2016) refined the eruption age for $^{40}Ar/^{39}Ar$-dated and tephra-constrained Holocene lava flows by comparing characteristic magnetization directions recorded in the lavas with a palaeosecular variation record based on lake sediments from Lake Mavora (South Island, New Zealand) independently calibrated using ^{14}C (Turner et al., 2015). Dating lava flows using palaeomagnetic directions, however, requires a previous eruption age constraint and is limited to the Holocene in New Zealand due to the extension of the sediment record. Only the ages of five flows were constrained using this method: one from the Crater Lake Member, three from the Iwikau Member (Delta Corner, Bruce Road and Taranaki Falls flows) and the western lobe of the Saddle Cone Member. Eruption ages provided by Greve et al. (2016) for the Crater Lake, Delta Corner and Bruce Road flows are tightly constrained (age ranges of *ca* 300 yrs), while their preferred ages for the Taranaki Falls flow and Saddle Cone Member span over ∼2 and ∼1.2 kyr, respectively (Table 1).

https://doi.org/10.5194/egusphere-2024-163
Preprint. Discussion started: 23 January 2024

Formation	Member (previous age constraints)		Eruption ages (± 2σ)	Methods	References	Sampled sites (this study)
Whakapapa (*<15 ka; postglacial*)	Crater Lake (*<5 ka*)		2400–2050 BP (0.2 ± 2.2 ka)	Palaeomagnetism (improved from $^{40}Ar/^{39}Ar$)	1, 2	-
	Iwikau	Tawhainui flows (*9–7 ka*)	8800–8500; 8200–7900 BP (6.0 ± 2.4 ka)	Palaeomagnetism (refined from $^{40}Ar/^{39}Ar$ and tephra stratigraphy)	1, 2	DC; WG; BR
		Mangatoetoenui flows (*<17 ka**)	9.2 ± 8.0; 0.8 ± 5.6 ka	$^{40}Ar/^{39}Ar$	2	LC; TSa; TSb; TFt
		Taranaki Falls flow (*11–9 ka**)	10 800–8900 BP (8.8 ± 2.8 ka)	Palaeomagnetism (improved from $^{40}Ar/^{39}Ar$)	1, 2	TFa
	Saddle Cone (*10–8 ka**)		9850–8650 BP	Palaeomagnetism (refined from tephra stratigraphy)	1	SCw-e; WP
	Pinnacle Ridge (*~10 ka**)		~10 ka	Correlation with tephra	3	PR
	Tureiti (*15–9ka*)		12.5 ± 2.6; 11.9 ± 2.8 ka	$^{40}Ar/^{39}Ar$	2	-
	Rangataua (*~15–10 ka**)		~15–10 ka	Stratigraphy	4, 5	RTp; RTm
	Paretetaitonga (*~15 ka*)		14.8 ± 3.0 ka	$^{40}Ar/^{39}Ar$	2	WT
	Turoa (*17–10 ka**)		15.1 ± 2.4; 11.9 ± 2.2 ka	$^{40}Ar/^{39}Ar$	2	MN; MS; CTa; CTb; TC
Mangawhero (*50–15 ka; synglacial*)	Makotuku (*24–16 ka*)		20.9 ± 2.8; 17.8 ± 2.2 ka	$^{40}Ar/^{39}Ar$	2	MF; NR; MA
	Waitonga (*25–21 ka*)		23.0 ± 1.6; 23 ± 8 ka	$^{40}Ar/^{39}Ar$	2, 6	-
	Te Piripiri (*~21 ka*)		21 ± 6 ka	$^{40}Ar/^{39}Ar$	6	-
	Horonuku (*29–15 ka*)		23 ± 4; 22 ± 7 ka	$^{40}Ar/^{39}Ar$	6	-
	Whakapapaiti (*~ 26 ka*)		25.7 ± 3.8 ka	$^{40}Ar/^{39}Ar$	2	-
	Manganuioteao (*36–22 ka*)		25.7 ± 2.6; 27.2 ± 4.8; 30.7 ± 5.2; 30.9 ± 2.2 ka	$^{40}Ar/^{39}Ar$	2	-
	Mananui (*42–38 ka*)		40.3 ± 2.2	$^{40}Ar/^{39}Ar$	2	-
	Te Kohatu (*44–36 ka*)		47.6 ± 1.4; 39.1 ± 1.4; 39.2 ± 2.0; 42.6 ± 1.8 ka	$^{40}Ar/^{39}Ar$	2	-
	Mangaturuturu (*46–36 ka*)		38.4 ± 2.4; 41.3 ± 1.8; 43.4 ± 2.4 ka	$^{40}Ar/^{39}Ar$	2	-
	Mangaehuehu (*47–40 ka*)		42.8 ± 1.0; 43.1 ± 1.4; 43.3 ± 1.6; 44.2 ± 1.8; 45.4 ± 2.0 ka	$^{40}Ar/^{39}Ar$	2	GR
	Ngahuinga (*48–35 ka*)		44.8 ± 3.0 ka	$^{40}Ar/^{39}Ar$	2	-
Waihianoa (*166–80 ka*)			88.1 ± 6.4; 95.9 ± 7.0; 119 ± 12; 120.7 ± 4.0; 121.4 ± 2.8; 121.7 ± 4.2; 129 ± 15; 130 ± 23; 131 ± 27; 133 ± 11; 133.6 ± 6.4; 134 ± 12; 135 ± 14; 138 ± 14; 147 ± 10; 147± 12; 154 ± 12 ka	$^{40}Ar/^{39}Ar$	2, 6	-
Te Herenga (*200–150 ka*)			158.8 ± 8.2; 169.4 ± 7.8; 174.6 ± 3.4; 183 ± 13; 186.2 ± 6.8; 187.9 ± 34.4; 197 ± 12; 205 ± 27 ka	$^{40}Ar/^{39}Ar$	2, 6	-

Table 1. Previous chronological studies from lava flows at Ruapehu. 1) Greve et al. (2016); 2) Conway et al. (2016); 3) Donoghue et al. (1999); 4) Price et al. (2012); 5) Eaves et al. (2016b); 6) Gamble et al. (2003). *Age limits redefined in this study based on $^{3}He_{cos}$ eruption ages.

https://doi.org/10.5194/egusphere-2024-163
Preprint. Discussion started: 23 January 2024

Figure 2. Examples of targeted sites. a) Large tumuli, 1.5 m above ground level (red arrow pointing to a 20 cm long GPS on flow top), GR site. b) Detail of lava top. Rough, irregular surfaces resembling 'a'ā lava flow morphologies, indicatives of minimal erosion, at site MN.

3 Methods

3.1 Sampling site selection

The selection of an adequate sampling site is an important step for cosmogenic nuclides exposure dating. Evidence of negligible erosion is essential, as well as confidence that the targeted rock has not been covered by other rocks, soil, ice, volcanic ash or vegetation for a significant amount of time since formation. For lava flows, effective sampling was achieved by targeting tumuli, spikes and other features standing above the main flow surface (e.g. Anderson et al., 1994; Licciardi et al., 2006) which preserve characteristic primary cooling morphologies of flow surfaces (Figure 2).

Using aerial photographs and digital elevation models (DEMs) based on aerial imagery and a newly acquired LiDAR dataset, we revised the existing maps (Townsend et al., 2017) and identified individual lava flows within each of the different members of the Whakapapa Formation, which we then targeted in our sampling (Figure 4). Lack of adequate lava surface exposures did not permit us to sample lavas from the Tureiti and Crater Lake members. Due to the lack of chronological data on several lavas

https://doi.org/10.5194/egusphere-2024-163
Preprint. Discussion started: 23 January 2024

of the Makotuku Member of the Mangawhero Formation (24–16 ka; Conway et al., 2016, Table 1), we additionally targeted three flows of this unit on outcrops outside of the LGM ice limits (MF, NR, MA; Figure 1c). We also sampled a site (GR) that we consider to be postglacial due to the presence of original (non-eroded) lava surfaces (Figure 2a) and its location inside the LGM ice limit of Barrell (2011, Figure 1c). Note that this exposure was previously mapped as Mangawhero Formation (Mangaehuehu Member) based primarily on its location on the volcano and similarity in appearance to nearby geochemically fingerprinted outcrops.

3.2 Sample collection

All samples were collected under a Research and Collection Permit of the Department of Conservation of New Zealand, obtained after a consultation process involving local Iwi (Māori tribes) with rightful claims to guardianship of Ruapehu. We sampled between three and six shallow surfaces (<6 cm below the flow top) for each targeted flow using a hammer and chisel. For recording the coordinates and altitude of each surface (vertical precision of 0.1 m) we used a differential Trimble Geo7X GPS corrected by data of VGMT (Ohakune, Land Information New Zealand) and the Chateau Observatory Base (GeoNet) stations. We also measured surface dip and orientation and azimuth-horizon angle pairs to account for topographic shielding. For the CTa, CTb and TC samples, *in situ* topographic shielding could not be acquired, so representative azimuth-horizon angle pairs were selected based on observations of DEMs. To test the accuracy of this approach, we compared values derived from DEMs to field-obtained shielding factors from other sites, showing an agreement of 95–99%.

3.3 Mineral separation

For each sample fragment used, mean thickness was calculated using a caliper in 5–40 points, and then a sample thickness average was obtained weighted by rock fragment mass. Afterwards, samples were crushed and sieved to obtain a 100–1000 μm size fraction, which was then rinsed to eliminate dust and organic matter and dried at 60° C.

Density separation was done using a 3.0 g/cm^3 sodium polytungstate solution, after which the heavy concentrates were leached in a HF 5%; NaOH 2.5% bath for 24 hours before immersing in HCl 3M to remove fluoride precipitates, following Bromley et al. (2014). After checking under a microscope, we leached a second and third time if necessary in HF 5%; NaOH 2.5% and/or HF 2.5%; NaOH 1.25%, until we achieved total removal of groundmass on most crystals. We then carried out magnetic separation of oxides and magnetic groundmass, and finally removed remaining impurities, based on colour and texture, to leave pure pyroxenes (olivines and pyroxenes in the GR samples).

3.4 Geochemical analyses

For each studied lava flow, major and trace element compositions were analysed at the Service d'Analyse des Roches et Minéraux (SARM) of the Centre de Recherches Pétrographiques et Géochimiques (CRPG, Université de Lorraine, Nancy, France) by inductively coupled plasma optical emission spectroscopy (ICP-OES) and inductively coupled plasma mass-spectrometry (ICP-MS), respectively, both for bulk rock and pure pyroxenes/olivines.

https://doi.org/10.5194/egusphere-2024-163
Preprint. Discussion started: 23 January 2024

3.5 Measurement of Helium isotopes concentrations

We analysed ^{3}He and ^{4}He concentrations in pyroxenes and olivines using a GV Instruments Helix Split Flight Tube multi-collector noble gas mass spectrometer attached to a gas line at CRPG (e.g. Schimmelpfennig et al., 2011; Blard et al., 2013, 2015).

Pure minerals were wrapped in tin capsules, loaded in a carousel and baked for one night at 100° C under ultrahigh vacuum. The samples were heated to >1300° C for 15 minutes in a full metal induction furnace (Zimmermann et al., 2018) and gases expelled were purified using four activated charcoal traps at 77 K in order to trap large amounts of CO_2, H_2O, N_2 and heavy noble gases (Ar, Kr and Xe) from the melted samples by physisorption. In parallel, four getters initially activated at 800° C were used at room temperature to trap all reactive species (e.g. H_2O, CO_2, N_2, O_2) by chemisorption. After these two steps, He was condensed using a cryogenic cold trap at 12 K, and then released at 75 K towards the mass spectrometer that measured, in static mode, ^{3}He and ^{4}He. The source settings were adjusted to get the best compromise between linearity, sensibility and stablity (e.g. ^{4}He sensitivity = 7.45 x 10^{13} $\pm$ 2% mV/mol, ^{3}He sensitivity = 4.30 x 10^{18} $\pm$ 5% cps/mol). HESJ gas standards (R/Ra = 20.63; Matsuda et al., 2002) were measured daily and ^{4}He and ^{3}He values were also routinely compared with CRONUS-P standards (Blard et al., 2015; Schaefer et al., 2016). The main source of background He (typical ^{4}He blanks of 1.3 x 10^9 $\pm$ 1.8 x 10^8 atoms; typical ^{3}He blanks < 5 x 10^3 $\pm$ 3.5 x 10^3 atoms;^{3}He/^{4}He ratios similar to 1 Ra) was the Ta crucible, which was degassed at 1800° C for 30 minutes prior to analyses.

3.6 Surface exposure age determinations

3.6.1 Calculation of cosmogenic ^{3}He

To correctly determine the concentration of ^{3}He$_{cos}$, it is necessary to consider the non-cosmogenic contributions to total ^{3}He measured when fused in vacuo (^{3}He$_{tot}$), described by the equation:

$$^3He_{tot} = {}^3He_{cos} + {}^3He_{atm} + {}^3He_{nuc} + {}^3He_{mag} \quad (1)$$

where ^{3}He$_{atm}$ is the atmospheric ^{3}He hosted at the minerals' surfaces as a contaminant and is time independent. ^{3}He$_{nuc}$ is the nucleogenic ^{3}He produced by capture of low-energy neutrons emitted by ^{6}Li and dependent on Li concentrations in the mineral, U and Th concentrations in the rock, and the mineral closure age (equivalent to eruption age for pyroxenes and olivines in volcanic rocks; Kurz, 1986). ^{3}He$_{mag}$ is the magmatic ^{3}He contribution (time independent) present in melt and fluid inclusions, and within the minerals' matrix.

Atmospheric He (both ^{3}He and ^{4}He) concentrations are inversely proportional to the mineral grain size and become insignificant for minerals larger than 100 μm (Blard, 2021), so they was considered non-existent in our calculations. ^{3}He$_{nuc}$ quotas are normally negligible for uneroded lava flows, in which the closure and exposure ages are the same (Kurz, 1986), as shown by our calculations (Table A3) based on the spreadsheet developed by Blard (2021).

https://doi.org/10.5194/egusphere-2024-163
Preprint. Discussion started: 23 January 2024

The total contribution of $^3He_{mag}$ was estimated based on magmatic $^3He/^4He$ ratios measured in pyroxene and olivine phenocrysts in the Waimarino and Ohakune basalts ($7.5 \pm 1.5 \times 10^{-6}$) by Patterson et al. (1994) and corrected from $^3He_{tot}$ using Equation 3.

The total amount of ^4He measured in each sample ($^4He_{tot}$) is defined by the equation:

$$^4He_{tot} = {}^4He_{mag} + {}^4He_{atm} + {}^4He_{rad} + {}^4He_{cos} \quad (2)$$

where $^4He_{mag}$ corresponds to the time independent magmatic ^4He quota naturally present in the minerals, while $^4He_{atm}$ accounts for atmospheric ^4He contaminating the minerals' surfaces (time independent). $^4He_{rad}$ is radiogenic ^4He generated by the decay of radioactive isotopes such as U, Th and Sm present in the minerals and dependent on the abundance of these elements in the minerals, and the closure age. Crystals normally exhibit an enriched ^4He exterior rim generated by implanted $^4He_{rad}$ from the matrix (Lal, 1989), typically with higher concentrations of U, Th and Sm. $^4He_{cos}$ refers to the cosmogenic contribution of ^4He, negligible compared to other non-cosmogenic varieties of ^4He (Blard, 2021) and are therefore also omitted from our calculations.

In this paper we follow the approach of Blard and Farley (2008), which corrects for the contributions of $^4He_{rad}$, $^4He_{mag}$ and $^3He_{mag}$ for uneroded lava flows, using the equation:

$$^3He_{cos} = \frac{^3He_{tot} - {}^4He_{tot}\left(\frac{^3He}{^4He}\right)_{mag}}{R} \quad (3)$$

where R (or R factor) is defined by:

$$R = 1 - \left(\frac{P_4}{P_3}\right)\left(\frac{^3He}{^4He}\right)_{mag} \quad (4)$$

where P_4 and P_3 are the $^4He_{rad}$ and local $^3He_{cos}$ production rates.

Individual values of P_4 were calculated for each lava flow using the spreadsheet developed by Blard (2021), neglecting the implanted $^4He_{rad}$ component to account for the removal of the ^4He-enriched crystal rim with HF leaching.

Sample-specific P_3 estimates were obtained following the Lal-Stone time corrected scaling scheme (Lal, 1991; Stone, 2000; Nishiizumi, 1989; Balco et al., 2008) using the online calculator 'Cosmic Ray Exposure program' (CREp, https://crep.otelo.univ-lorraine.fr/; Martin et al., 2017) and the global $^3He_{cos}$ production rate database therein.

3.6.2 Determination of exposure ages

To obtain exposure ages, we used the CREp online calculator, which calculated exposure ages based on our $^3He_{cos}$ concentrations and scaling parameters, Lal-Stone time corrected scaling scheme (Lal, 1991; Stone, 2000; Nishiizumi, 1989; Balco et al., 2008), ERA40 atmosphere model (Uppala et al., 2005), the geomagnetic framework of Muscheler et al. (2005) and world wide mean $^3He_{cos}$ production rates of 122 ± 12 at/g/yr at sea level on high latitudes (SLHL). This production rate value is supported by a local calibration test using the radiocarbon-dated debris avalanche deposits of the Murimotu Formation, on the outer northwestern slopes of Ruapehu (Eaves et al., 2015). Exposure ages calculated using the LSD scaling scheme (Lifton

https://doi.org/10.5194/egusphere-2024-163
Preprint. Discussion started: 23 January 2024

et al., 2014) and different atmospheric models and geomagnetic databases are available in the supplementary material, showing variations of 1–3% compared with the exposure ages caculated using the parameters outlined above. This is, however, not the case of the LSD geomagnetic framework, which provides exposure ages between 8.6 and 3.8% younger. This discrepancy can be explained by a higher spatial variability of the LSD framework than other models, and especially by the model's relative scaling factor high over the New Zealand region during the Holocene (Lifton, 2016). New paleosecular variation records based on New Zealand lake sediment cores (Turner et al., 2015; Turner and Corkill, 2023) suggest that this scaling factor high is a spatial artefact caused by the small number of Southern Hemisphere records used to make up the global model on the LSD framework. Thus, we place greater emphasis on results produced using models that do not contain such effects (e.g. Muscheler et al., 2005; Lifton, 2016).

We measured three to five samples per lava flow to counter the possibility that individual samples may be affected by erosion or shielding that would compromise their accuracy for constraining the time of lava flow emplacement. To derive single exposure ages for lava flows from these multiple measurements, we used each sample's internal 1σ (output from CREp, without including the P_3 uncertainty) and implemented the summary age statistics and outlier removal routine contained in version 3 of the Balco et al. (2008) online exposure age calculator, fully described in the documentation (section 4.C. available at https://sites.google.com/a/bgc.org/v3docs/). In summary, we used weighted mean summary ages if the samples formed a single population at the 95% confidence interval using the chi-squared statistic. If this result could not be achieved by incremental outlier removal while maintaining a sample population $\geq$3, then we used the mean and standard error as the summary age of the lava flow. We finally propagated the P_3 uncertainty into all summary ages, which we report with their 2σ interval. In the case of flows for which less than three samples passed the single population test (or only two samples were analysed), we considered the summary age to be a minimum eruption age. For those flows with three or more exposure ages passing this test, summary ages were considered robust eruption ages. We used internal 2σ intervals (INT 2σ, which do not include P_3 errors) to compare intra and inter-site age distributions and clustering.

4 Results

4.1 Bulk rock and mineral geochemistry

Major and trace elements concentrations of bulk rocks and minerals fom each of the lava flows studied can be found in Table A2.

All bulk rock analyses yielded basaltic andesite to andesitic compositions according to the classification scheme of Le Maitre (2002). Our results indicate that, from the sampled flows, younger flows tend to be less evolved than older flows (Figure A1).

Most flows yielded a bulk geochemistry similar to the reported ranges (Conway et al., 2016) for the respective units they were classified as (Townsend et al., 2017). The only exception is the site here referred as NR, which shows higher MgO (6.22 wt.%) and lower Na_2O (2.95 wt.%) than other samples of the Makotuku Member (2-3 wt.% and 3.4–4 wt.%, respectively; Conway et al., 2016). Instead, major element geochemistry of our NR sample matches that of the Mangaehuehu Member (4.7–7 wt.% MgO and 3-3.4 wt.% Na_2O; Conway et al., 2016), the lavas of which are significantly older (Table 1).

https://doi.org/10.5194/egusphere-2024-163
Preprint. Discussion started: 23 January 2024

Mineral geochemistry shows that, on average, the pyroxenes are pigeonite (Figure 3a), although analyses of modal phases of Ruapehu lavas (Hackett, 1985; Conway, 2016) suggest that this represents a combination of augite and enstatite crystals. MN and TSa yield average compositions of enstatite phases, indicating that the orthopyroxene phase dominates over the clinopyroxene in these flows. The analysed olivines (sample GR) are magnesium-rich (Fo^{69}; Table A2).

In general, trace element concentrations are relatively homogeneous across the sampled sites. Figure 3b shows the concentrations of the main radioactive elements producing $^4He_{rad}$ (U, Th and Sm) in bulk rock and in the mineral phases (pyroxenes and olivines). Bulk rock analyses yielded values of 0.94–1.74, 4.04– 6.50 and 2.41–3.25 ppm of U, Th, and Sm, respectively. Pyroxenes contain 0.01–0.10, 0.04–0.36, and 0.44–2.07 ppm, respectively (uncertainties <20% and detection limits of 0.01 ppm). GR olivines have lower contents of these elements (with U below the detection limit), and therefore larger P_4 associated errors. Note that U and Th concentrations in the rock are not involved in the production of the measured $^4He_{rad}$, as the external crystal rims were removed before the analyses.

4.2 Helium isotopes and cosmogenic ^{3}He concentrations

We analysed a total of 80 samples from 23 individual flows. All ^{3}He and ^{4}He measurements are shown in Table 2. Measured ^{3}He varies between 2.1 x 10^6 and 2.4 x 10^7 at/g, with 2–7% of relative associated error (1σ). $^4He_{tot}$ values typically range between 0.3 and 9.6 x 10^{10} at/g with uncertainties between 0.04 and 0.18 x 10^{10} at/g.

The complete detail of all sources of corrections is available in Table A3, being the magmatic He the most impactful on $^3He_{cos}$ corrections in our samples. Calculated $^3He_{nuc}$ production rates (P_{nuc}) are four orders of magnitude below P_3 values, making $^3He_{cos}$ results insensitive to nucleogenic corrections. P_4 ranges between 4 x 10^4 and 3 x 10^5 at/g/yr. We assume a 10% error associated with all P_4 results, except for the site GR, which has lower concentrations of radioactive elements (hence, the lowest P_4 number within our lavas) with uncertainties of 20-40%, for which we considered a 25% in our P_4 estimates, and consider a magmatic $^3He/^4He$ ratio (7.5 ± 1.5 x 10^{-6}) based on ratios measured in clinopyroxenes of the Ohakune and Waimarino basalts (Patterson et al., 1994). This ratio, combined with our P_4 calculations (3.5 x 10^4–6.1 x 10^5 at/g/yr) and local P_3 values between 313 and 584 at/g/yr (elevations between 1288 and 2148 m asl) yields R factors >0.99, indicating that corrections for $^4He_{rad}$ has a minor (<1%) impact on our final $^3He_{cos}$ values. Uncertainties of 20% associated with our chosen $^3He/^4He_{mag}$ ratio represent *ca* 5% of the informed error associated with $^3He_{cos}$ results. Our samples' $^3He_{cos}/^3He_{tot}$ ratios vary between 0.90 and 0.99, implying that the $^3He_{cos}$ quota dominates over nucleogenic and magmatic ^{3}He.

4.3 Surface exposure and eruption ages

We obtained 16 eruption ages and seven minimum eruption ages based on the criteria defined in Section 3.6.2 (Table 2).

https://doi.org/10.5194/egusphere-2024-163
Preprint. Discussion started: 23 January 2024

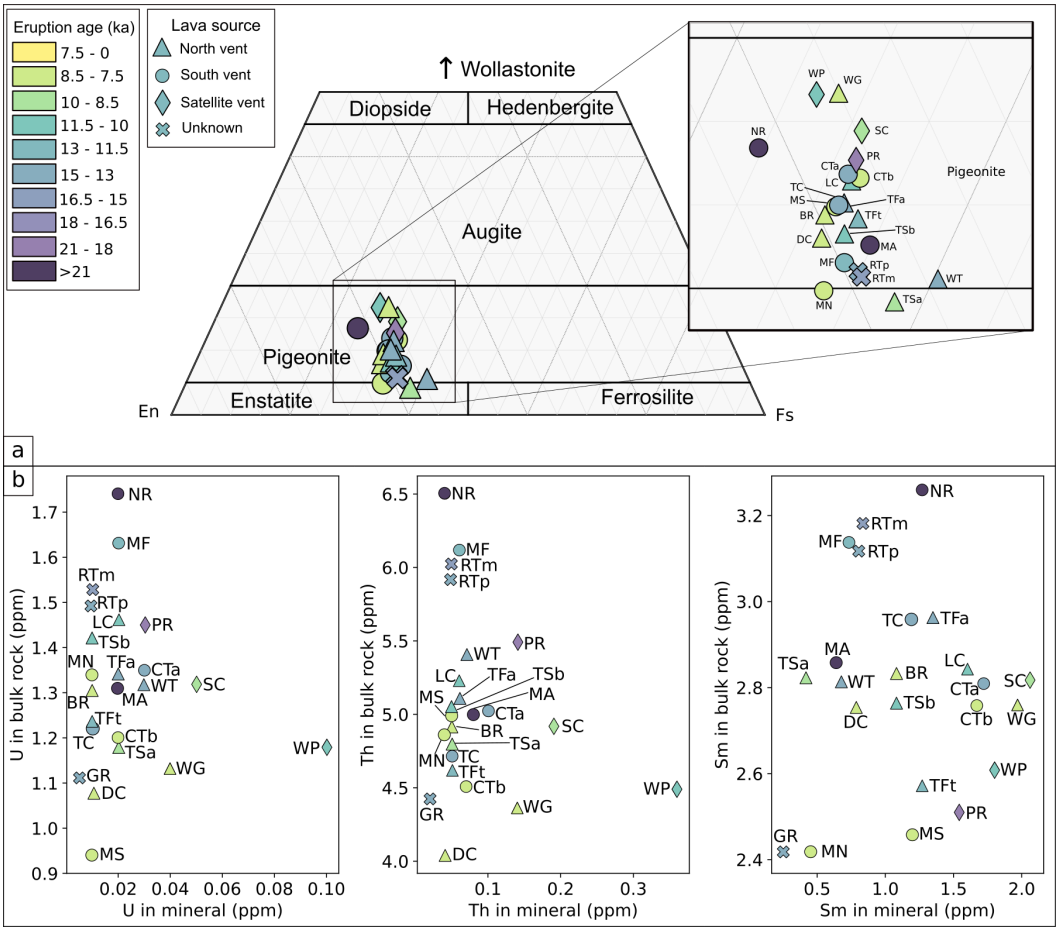

Figure 3. a) Pyroxene compositions according to the classification scheme of Morimoto et al. (1988). Each triangle represents the average geochemistry of each lava flow's pyroxene population. b) U, Th and Sm concentrations in the samples. x axis represents concentrations in minerals (pyroxenes and olivines) and y axis in bulk rock.

4.3.1 Iwikau Member

The Iwikau Member of the Whakapapa Formation covers a large area on the northwestern and eastern flanks of Ruapehu (Figure 1), and is subdivided into three flow packages: Tawhainui, Mangatoetoenui, and Taranaki Falls flows (Figure 4a, b), all interpreted to have originated from Ruapehu's northern vent (Townsend et al., 2017).

Tawhainui Flows

The Tawhainui Flows comprise a voluminous sequence of lava flows on the northwestern slopes of the volcano. They have been the most studied unit of Ruapehu due to its accessibility and availability of the fresh exposures of flow interiors, facilitated by the construction of the largest ski field in New Zealand's North Island. We sampled three flows from this unit: Delta Corner flow (DC samples), Bruce Road flow (BR samples, both after Greve et al., 2016) and Whakapapa Glacier flow (WG samples).

https://doi.org/10.5194/egusphere-2024-163
Preprint. Discussion started: 23 January 2024

The fresh-looking Delta Corner flow (that has distinct 'a'ā surface morphologies) yielded well clustered exposure ages, from which we obtained an eruption age of 7.8 ± 1.5 ka. The Whakapapa Glacier flow is one of the youngest lavas of the sequence based on stratigraphic relations, which suggest a comparable age to that of the Delta Corner flow. Due to the highly eroded nature of the flow's surface, only two WG samples were collected, which yielded a minimum eruption age of 7.8 ± 2.4 ka, consistent with the age of the Delta Corner flow. The Bruce Road flow is a large 'a'ā flow that underlies the Delta Corner flow. Downslope from the BR sample site, the flow has unclear boundaries, as it is covered by vegetation. Based on three individual exposure ages, we obtained an eruption age of 8.0 ± 2.1 ka for the Bruce Road flow.

Mangatoetoenui Flows

This subunit includes a group of lava flows on the eastern slopes of Ruapehu and its age is poorly constrained (Table 1). We sampled four individual flows classified based on geochemistry and location within the Mangatoetoenui Flows: Lava Cascade (LC), Tukino Slopes-a (TSa), Tukino Slopes-b (TSb) and Tukino Flats (TFt; Figure 4b).

The LC site is interpreted to be part of a *ca* 4-km long lava flow described in detail by Rhodes (2012), terminating on a 20 m high lava cascade at 1620 m asl. We analysed four individual samples from an outcrop located *ca* 1 km upslope from the lava toe and obtained an eruption age of 11.4 ± 2.3 ka, with one young outlier removed (sample LC256). The outlier can be explained by local erosion, shielding from a now collapsed neighboring lava tumuli (and hence an underestimation of the shielding factor) or a period of tephra cover that could have reduced the ^{3}He production on the surface of LC256.

The Tukino Slopes-a flow had not been previously dated, but its location and stratigraphic position suggest a similar eruption age to LC and TSb. All measured TSa samples (8.7, 9.5 and 9.8 ka) form a single population and provide an eruption age of 9.4 ± 1.8 ka, in good agreement with the stratigraphy.

TSb sample site likely corresponds to the same flow as sample CC569 dated at 9.2 ± 8.0 by Conway et al. (2016). Our exposure ages of 10.5, 11.9, and 11.9 ka result in a refined eruption age of 11.5 ± 2.2 ka for this flow.

Based on three individual exposure ages of 7.7, 10.7 and 7.3 ka (that do not form a single population), we obtained a minimum eruption age of 8.6 ± 4.6 ka for the Tukino Flats flow. The older exposure age (10.7 ka) is difficult to explain as an outlier, as the presence of inherited ^{3}He is not justifiable for lava flows, whereas the younger ages may be explained as outliers owing to surface erosion or temporal burial by alluvium or tephra.

Taranaki Falls flow

The Taranaki Falls flow (TFa) is an elongated lava flow which outcrops discontinuously for *ca* 8 km almost directly to the north of the volcano's summit area (Townsend et al., 2017, Figure 4a) and terminates on the 20 m waterfall after which it is named. We sampled the flow at an outcrop 800 m upstream from the flow terminus and obtained exposure ages of 14.5, 14.2, and 15.0 ka, resulting in an eruption age of 14.6 ± 2.9 ka.

4.3.2 Saddle Cone Member

This unit comprises a large, lobate 'a'ā flow originating from a parasitic cone on the north-northeastern side of Ruapehu, almost disconnected from the main edifice (Figure 4a). It also includes a smaller blocky lava flow lying between this cone and

https://doi.org/10.5194/egusphere-2024-163
Preprint. Discussion started: 23 January 2024

Ruapehu's summit region (likely originated from a satellite vent), adjacent to the Waihohonu Ridge and here referred to as the Waihohonu Plateau lavas (WP), linked to the main Saddle Cone deposits by its geochemical similarity and location.

The age of samples from the main western lobe of the Saddle Cone lavas (SCw; 10.3, 10.0 and 9.4 ka) show good agreement. We additionally analysed a sample from the eastern lobe (SCe, whose surface elevation is more than 100 m below that of the main lobe) to test the hypothesis of a multi-episodic origin. The obtained exposure age of this sample is 9.6 ka (Table 2), indistinguishable from those of the western lobe. We suggest a single eruption age for both lobes of 9.8 ± 2.0 ka (n=4).

The blocky nature of the Waihohonu Plateau flow made it difficult to find uneroded surfaces, and only two samples were obtained. Analyses from these samples yield a minimum eruption age of 11.0 ± 2.2 ka, which represents the first date for this flow other than an estimation of *ca* 8.5–10 ka based on the geochemical similarity with other Saddle Cone lavas (Townsend et al., 2017).

4.3.3 Pinnacle Ridge Member

The Pinnacle Ridge Member is a welded spatter deposit linked to a dike on a ridge of the same name on the northern flanks of the volcano (Figure 4a). PR samples yielded exposure ages of 20.6, 18.8 and 21.3 ka, resulting in an eruption age of 20.2 ± 3.9 ka for this unit, suggesting that the deposit was emplaced during the LGM.

4.3.4 Rangataua Member

The Rangataua Member includes the longest and most voluminous known lava flow of Ruapehu (≥15 km long; ∼1.5 km^3). It first outcrops *ca* 3.5 km south from the summit, which led to the hypothesis that it is sourced from a satellite vent (Hackett, 1985; Price et al., 2012), although Townsend et al. (2017) suggest initial transport over ice as a possible alternative explanation for its rootless nature. Based on geochemical differences, this unit was first subdivided by Price et al. (2012) into proximal, medial and distal flows. We sampled the Rangataua Member (RT) two locations; one close to the highest outcrops (RTp, "proximal"), and another one *ca* 1 km to the south (RTm, "medial"). We did not sample the distal flows due to vegetation cover (Figure 1c), which are interpreted to be older than the medial flows.

Results of RTm samples (16.1, 16.0, 15.2 and *8.1* ka) include a young outlier, but the remaining samples are internally consistent and indicate an eruption age of 15.7 ± 3.0 ka. RTp samples yielded exposure ages of 13.8, 12.3, 13.8 and 14.3 ka and a final eruption age of 13.5 ± 2.6 ka, which agrees with the field relationships of the area, as this flow overlies RTm. The ages of the Rangataua medial and proximal flows and their INT 2σ uncertainties (15.7 ± 0.8 and 13.5 ± 0.6, respectively) do not overlap, indicating that they correspond to different eruptive episodes.

4.3.5 Paretetaitonga Member

The Paretetaitonga Member comprises a series of lava flows that likely originated from the northern summit vent of Ruapehu and emplaced in the headwaters of the Whakapapaiti Stream, northwest of the summit area (Figure 4a). We sampled one flow

https://doi.org/10.5194/egusphere-2024-163
Preprint. Discussion started: 23 January 2024

(Whakapapaiti, WT samples) and obtained exposure ages that agree with each other (12.8, 13.4 and 13.7 ka), resulting in an eruption age of 13.3 ± 2.6 ka.

4.3.6 Turoa Member

The Turoa Member corresponds to a sequence of numerous flows extending directly west from the edge of Ruapehu's crater rim and reaching the Mangaturuturu valley bottom. Based on the distributions of the flows, this unit is assumed to have been formed by effusive activity from the southern summit vent. We sampled five sites, distributed on the northern (MN, MS), central (CTa, CTb) and western (TC) areas (Figure 4c) covered by this unit.

The Mangaturuturu North flow (MN) corresponds to a flow on the headwaters of the Mangaturuturu Stream, and due to stratigraphic relations and flow morphologies was suspected to be the youngest lava on western Ruapehu. We analysed five surfaces of this flow (8.0, 8.8, *6.0*, 8.9 and 7.7 ka), and eliminating the young outlier of 6.0 ka, they yield a robust eruption age of 8.3 ± 1.6 ka.

Poor exposures of original flow surfaces prevented us from collecting more than three samples from the Mangaturuturu South (MS) flow. Additionally, purification of the minerals in these samples was incomplete due to high (>50%) mass loss with each HF leaching cycle, and we suspect an overestimation of measured pyroxene mass for these samples. Sample analyses resulted in exposure ages that did not pass the single population test (Table 2), providing a minimum eruption age of 6.1 ± 1.7 ka.

Central Turoa a/b (CTa/CTb) flows are located in close proximity to each other and at a similar elevation, south of the MN and MS sites. However, our analyses indicate that these two flows correspond to two different eruptive episodes. We only collected two samples from the CTa flow due to a lack of suitable surfaces, which suggest a minimum eruption age of 13.5 ± 2.7 ka. Three out of four CTb samples analysed (exposure ages of *4.9*, 8.8, 8.4 and 8.4) show good agreement and yield an eruption age of 8.5 ± 1.7 ka.

The TC site is part of a large flow reaching the Mangaturuturu River valley floor. Individual exposure ages (*11.3*, 14.1, 13.0 and 13.2 ka) include a young outlier and indicate an eruption age of 13.4 ± 2.6 ka for the Turoa Cascades flow.

4.3.7 Makotuku Member (Mangawhero Formation)

We sampled three flows previously mapped as part of the Makotuku Member of the Mangawhero Formation; Makotuku Flat (MF) on the southwest, and Ngā Rimutāmaka and Makahikatoa (NR and MA, named after local site and stream, respectively) on the south of Ruapehu's edifice. The spatial distribution of Makotuku lavas suggest that they originated from the southern summit vent.

Although results of analyses of MF samples are not particularly well clustered, they behave as a single population and provide an eruption age of 12.5 ± 3.5 ka.

Analyses of NR samples yield well clustered exposure ages, and we interpret an eruption age of 42.9 ± 8.6 ka, which corresponds to the only date provided for this lava flow so far. It is worth noting that this age and the geochemical composition of this flow match with the ^{4039}Ar ages and high-MgO/low-Al_2O_3 nature of Mangaehuehu Member lavas (Table 1).

https://doi.org/10.5194/egusphere-2024-163
Preprint. Discussion started: 23 January 2024

The small area where the Makahikatoa flow outcrops prevented us from obtaining more than two suitable samples, which yielded a minimum eruption age of 53.7 ± 17.4 ka and are the first age constraints for this flow.

4.3.8 Mangaehuehu Member (Mangawhero Formation)

We sampled a lava flow (Girdlestone Ridge, or GR) outcropping on a ridge top *ca* 1.5 km south from Ruapehu's summit and 800 m southwest from Girdlestone peak. This site was previously mapped as Mangaehuehu Member lavas (Townsend et al., 2017) based on interpretation of aerial imagery. However, the rubbly nature of the flow's surface observed in the field during this study suggest that it could be younger than previously interpreted. The mineral separation process applied to all samples produced the only olivine concentrate (with a minor pyroxene population) of this study.

Analyses of these samples indicate a minimum eruption age of 12.7 ± 5.3 ka, which represents the first age constraint for this lava flow.

https://doi.org/10.5194/egusphere-2024-163
Preprint. Discussion started: 23 January 2024

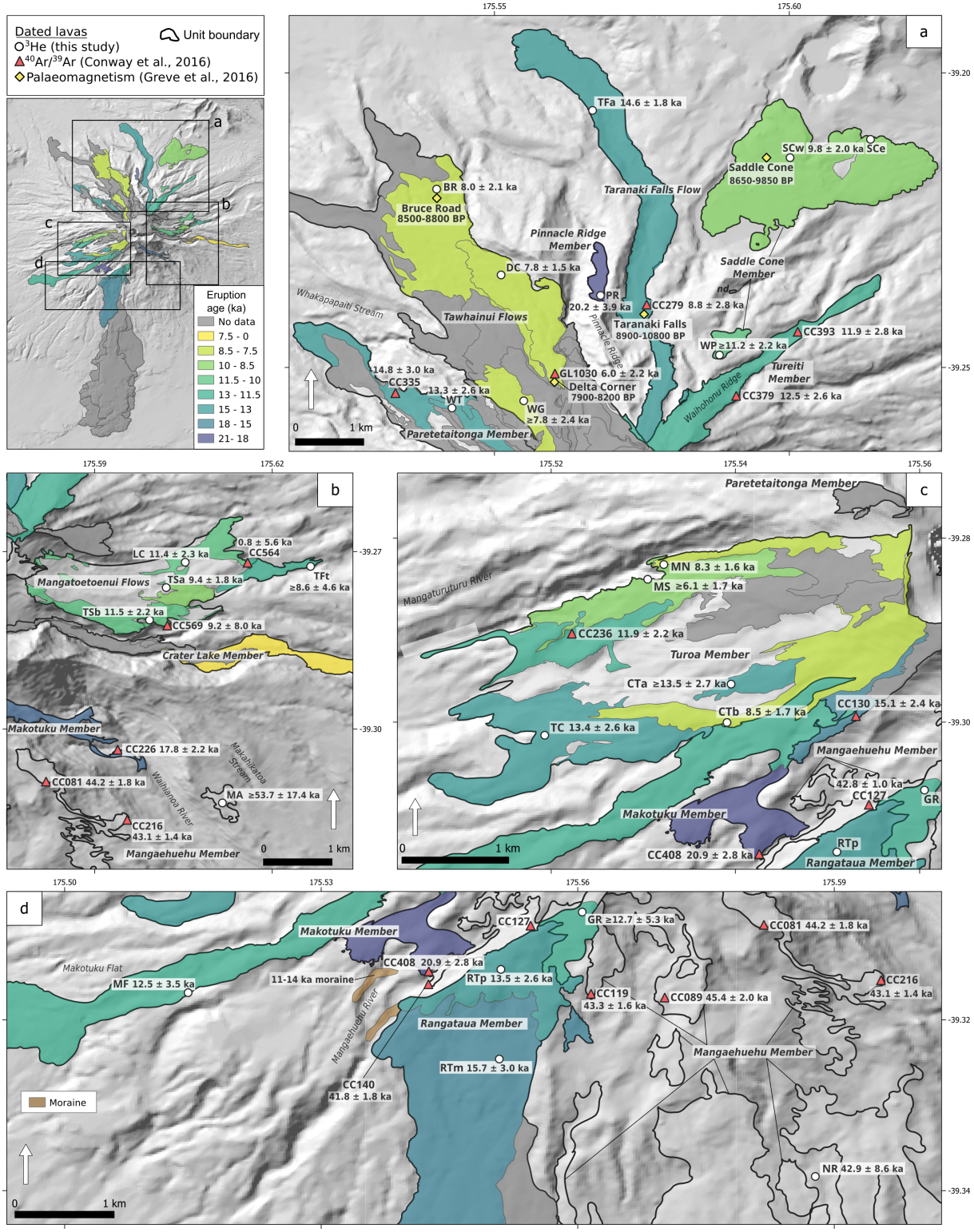

Figure 4. Map of dated <21 ka lava flows on: a) northern, b) eastern, c) western, d) southern Ruapehu. Polygons redefined from Townsend et al. (2017). Boundaries of the Mangaehuehu Member (Mangawhero Formation) as of Townsend et al. (2017) shown for context of site NR of this study. Grey polygons represent postglacial flows without chronological data.

https://doi.org/10.5194/egusphere-2024-163
Preprint. Discussion started: 23 January 2024

Table 2: Results of Helium isotopes measurements and exposure ages by sample.

Sample	Latitude (S)	Longitude (E)	Elevation (MSL)	Shielding factor	$^{3}He_{tot}$ $\pm1\sigma$ (10^{6}at/g)	$^{4}He_{tot}$ $\pm1\sigma$ (10^{10}at/g)	$^{3}He_{cos}$ $\pm1\sigma$ (10^{6}at/g)	Exposure age $\pm1\sigma$ (ka)
DC	*Tawhainui flows - Iwikau Member*						*Eruption age: 7.8 ± 1.5 ka (INT 2σ: 0.6 ka); n=3*	
327	39.235	175.552	1600.4	0.999	2.82 ± 0.21	0.72 ± 0.05	2.77 ± 0.21	7.49 ± 0.49
329	39.234	175.551	1591.8	0.999	3.08 ± 0.23	0.98 ± 0.05	3.01 ± 0.23	8.18 ± 0.56
330	39.234	175.551	1590.3	0.999	2.89 ± 0.22	0.80 ± 0.05	2.83 ± 0.22	7.69 ± 0.52
WG	*Tawhainui flows - Iwikau Member*						*Minimum eruption age: 7.8 ± 2.4 ka (INT 2σ: 2.0 ka); n=2*	
325	39.256	175.555	2079.1	0.991	4.44 ± 0.22	0.91 ± 0.05	4.39 ± 0.22	8.49 ± 0.39
326	39.256	175.555	2066.7	0.995	3.67 ± 0.19	1.15 ± 0.07	3.60 ± 0.19	7.10 ± 0.33
BR	*Tawhainui flows - Iwikau Member*						*Eruption age: 8.0 ± 2.1 ka (INT 2σ: 1.5 ka); n=4*	
014	39.220	175.541	1360.0	0.999	2.33 ± 0.12	0.61 ± 0.05	2.29 ± 0.13	7.34 ± 0.35
016	39.220	175.538	1359.2	0.982	2.57 ± 0.14	1.45 ± 0.06	2.47 ± 0.14	7.98 ± 0.40
017	39.219	175.541	1332.6	0.998	2.47 ± 0.14	1.65 ± 0.08	2.35 ± 0.14	7.67 ± 0.41
018	39.219	175.541	1332.4	0.998	2.87 ± 0.16	1.14 ± 0.08	2.79 ± 0.16	9.07 ± 0.50
LC	*Mangatoetoenui flows - Iwikau Member*						*Eruption age: 11.4 ± 2.3 ka (INT 2σ: 0.8 ka); n=3*	
254	39.272	175.605	1827.1	0.997	5.13 ± 0.36	1.22 ± 0.05	5.05 ± 0.37	11.34 ± 0.75
255	39.272	175.605	1826.6	0.997	5.01 ± 0.36	1.75 ± 0.06	4.89 ± 0.36	11.10 ± 0.73
256	39.272	175.605	1825.6	0.996	3.99 ± 0.29	1.46 ± 0.05	3.89 ± 0.29	8.97 ± 0.62 *
257	39.272	175.605	1824.7	0.996	5.28 ± 0.33	0.89 ± 0.72	5.22 ± 0.34	11.61 ± 0.69
TSa	*Mangatoetoenui flows - Iwikau Member*						*Eruption age: 9.4 ± 1.8 ka (INT 2σ: 0.5 ka); n=3*	
205	39.276	175.602	1905.1	0.983	3.98 ± 0.22	0.51 ± 0.10	3.95 ± 0.22	8.37 ± 0.46
206	39.276	175.602	1905.9	0.997	4.41 ± 0.24	0.14 ± 0.08	4.41 ± 0.24	9.51 ± 0.48
207	39.276	175.602	1905.5	0.997	4.61 ± 0.23	0.55 ± 0.06	4.58 ± 0.23	9.83 ± 0.46
TSb	*Mangatoetoenui flows - Iwikau Member*						*Eruption age: 11.5 ± 2.2 ka (INT 2σ: 0.6 ka); n=3*	
209	39.282	175.599	1932.5	0.997	5.06 ± 0.15	0.00 ± 0.14	5.06 ± 0.31	10.46 ± 0.59
210	39.282	175.599	1935.0	0.989	5.86 ± 0.28	1.41 ± 0.10	5.76 ± 0.28	11.87 ± 0.54
211	39.282	175.599	1929.2	0.993	5.78 ± 0.28	0.80 ± 0.05	5.73 ± 0.28	11.87 ± 0.55
TFt	*Mangatoetoenui flows - Iwikau Member*						*Minimum eruption age: 8.6 ± 4.6 ka (INT 2σ: 4.3 ka); n=3, see text*	
212	39.273	175.626	1521.2	0.994	2.71 ± 0.20	0.95 ± 0.06	2.64 ± 0.20	7.67 ± 0.53
213	39.273	175.626	1522.0	0.998	3.86 ± 0.27	1.03 ± 0.04	3.79 ± 0.27	10.73 ± 0.71
214	39.272	175.627	1506.4	0.988	2.47 ± 0.14	0.68 ± 0.06	2.42 ± 0.14	7.25 ± 0.36
TFa	*Taranaki Falls flow - Iwikau Member*						*Eruption age: 14.6 ± 2.9 ka (INT 2σ: 1.0 ka); n=3*	
088	39.207	175.567	1308.2	0.999	4.65 ± 0.29	1.64 ± 0.06	4.54 ± 0.29	14.54 ± 0.84
090	39.207	175.567	1302.8	0.996	4.38 ± 0.27	1.01 ± 0.05	4.32 ± 0.27	14.20 ± 0.82
091	39.206	175.566	1288.2	0.999	4.69 ± 0.29	1.14 ± 0.04	4.62 ± 0.29	14.99 ± 0.84
SCw	*Saddle Cone Member*						*Eruption age: 9.8 ± 2.0 ka (INT 2σ: 0.7 ka); n=4*	
001	39.214	175.601	1439.0	0.998	3.85 ± 0.28	5.14 ± 0.12	3.49 ± 0.29	10.33 ± 0.79
002	39.214	175.601	1439.3	0.998	3.59 ± 0.26	3.03 ± 0.08	3.39 ± 0.27	10.04 ± 0.73
003	39.215	175.600	1443.3	0.998	3.45 ± 0.25	3.91 ± 0.09	3.18 ± 0.26	9.39 ± 0.70
SCe								
093	39.212	175.614	1308.18	0.993	2.97 ± 0.22	0.92 ± 0.05	2.93 ± 0.22	9.62 ± 0.68
WP	*Saddle Cone Member*						*Minimum eruption age: 11.2 ± 2.2 ka (INT 2σ: 0.6 ka); n=2*	
007	39.248	175.588	1911.7	0.996	5.63 ± 0.23	2.06 ± 0.07	5.59 ± 0.23	11.68 ± 0.44
008	39.248	175.588	1912.1	0.995	5.22 ± 0.22	1.94 ± 0.03	5.13 ± 0.23	10.77 ± 0.43

https://doi.org/10.5194/egusphere-2024-163
Preprint. Discussion started: 23 January 2024

Table 2: Continued.

Sample	Latitude (S)	Longitude (E)	Elevation (MSL)	Shielding factor	$^{3}He_{tot}$ $\pm1\sigma$ (10^{6}at/g)	$^{4}He_{tot}$ $\pm1\sigma$ (10^{10}at/g)	$^{3}He_{cos}$ $\pm1\sigma$ (10^{6}at/g)	Exposure age $\pm1\sigma$ (ka)
PR	*Pinnacle Ridge Member*						*Eruption age: 20.2 ± 3.9 ka (INT 2σ: 1.1 ka); n=3*	
083	39.237	175.567	1730.7	0.979	9.39 ± 0.44	6.56 ± 0.20	8.93 ± 0.45	20.62 ± 0.96
084	39.239	175.567	1860.9	0.988	9.42 ± 0.44	7.72 ± 0.24	8.87 ± 0.46	18.80 ± 0.88
085	39.239	175.567	1857.9	0.997	10.69 ± 0.49	5.84 ± 0.18	10.28 ± 0.50	21.31 ± 0.97
RTp	*Rangataua Member*						*Eruption age: 13.5 ± 2.6 ka (INT 2σ: 0.6 ka); n=4*	
027	39.314	175.551	1831.4	0.997	6.38 ± 0.25	1.74 ± 0.08	6.26 ± 0.25	13.83 ± 0.52
028	39.314	175.551	1833.1	0.996	5.73 ± 0.26	2.13 ± 0.12	5.58 ± 0.26	12.34 ± 0.55
029	39.314	175.551	1832.9	0.996	6.42 ± 0.36	2.24 ± 0.18	6.26 ± 0.37	13.81 ± 0.75
030	39.314	175.551	1816.4	0.988	6.45 ± 0.31	0.98 ± 0.06	6.38 ± 0.31	14.31 ± 0.62
RTm	*Rangataua Member*						*Eruption age: 15.7 ± 3.0 ka (INT 2σ: 0.8 ka); n=3*	
045	39.323	175.552	1585.9	0.991	6.30 ± 0.38	1.83 ± 0.07	6.17 ± 0.38	16.14 ± 0.90
046a	39.325	175.551	1567.6	0.979	6.14 ± 0.25	0.74 ± 0.05	6.09 ± 0.25	
046b	39.325	175.551	1567.6	0.979	5.98 ± 0.30	0.98 ± 0.08	5.91 ± 0.30	
046 mean	39.325	175.551	1567.6	0.979			6.03 ± 0.30	16.00 ± 0.64
047	39.325	175.550	1567.4	0.997	5.91 ± 0.29	1.13 ± 0.06	5.83 ± 0.29	15.24 ± 0.68
048	39.325	175.550	1567.3	0.997	3.08 ± 0.16	1.64 ± 0.07	2.96 ± 0.16	8.11 ± 0.40*
WT	*Paretetaitonga Member*						*Eruption age: 13.3 ± 2.6 ka (INT 2σ: 0.6 ka); n=3*	
073	39.257	175.543	1892.4	0.987	6.01 ± 0.28	0.35 ± 0.08	6.00 ± 0.28	12.78 ± 0.58
074	39.257	175.543	1892.5	0.991	6.36 ± 0.26	0.73 ± 0.04	6.32 ± 0.26	13.39 ± 0.54
075	39.256	175.541	1785.0	0.990	6.06 ± 0.26	1.24 ± 0.05	5.98 ± 0.27	13.70 ± 0.57
MN	*Turoa Member*						*Eruption age: 8.3 ± 1.6 ka (INT 2σ: 0.5 ka); n=4*	
217	39.283	175.532	1815.9	0.993	3.49 ± 0.24	0.30 ± 0.05	3.47 ± 0.24	7.98 ± 0.50
218	39.283	175.532	1813.9	0.993	3.82 ± 0.23	0.37 ± 0.04	3.80 ± 0.23	8.84 ± 0.51
219	39.283	175.532	1812.1	0.993	2.47 ± 0.19	0.42 ± 0.05	2.45 ± 0.19	5.98 ± 0.39 *
220	39.283	175.533	1817.5	0.993	3.91 ± 0.25	0.77 ± 0.03	3.88 ± 0.25	8.88 ± 0.54
221	39.283	175.533	1822.8	0.993	3.30 ± 0.20	0.08 ± 0.04	3.29 ± 0.20	7.65 ± 0.42
MS	*Turoa Member*						*Minimum eruption age: 6.1 ± 1.7 ka (INT 2σ: 1.4 ka); n=3, see text*	
222	39.285	175.530	1750.6	0.954	2.58 ± 0.16	0.50 ± 0.04	2.54 ± 0.16	6.65 ± 0.35
223	39.285	175.531	1751.4	0.992	2.51 ± 0.17	0.12 ± 0.05	2.50 ± 0.17	6.31 ± 0.36
224	39.285	175.531	1750.9	0.992	2.08 ± 0.16	0.40 ± 0.11	2.05 ± 0.16	5.32 ± 0.37
CTa	*Turoa Member*						*Minimum eruption age: 13.5 ± 2.7 ka (INT 2σ: 1.0 ka); n=2*	
229	39.296	175.540	1924.0	0.996	6.57 ± 0.33	2.35 ± 0.09	6.41 ± 0.34	13.17 ± 0.66
230	39.296	175.540	1925.1	0.996	6.93 ± 0.36	2.76 ± 0.11	6.74 ± 0.36	13.81 ± 0.69
CTb	*Turoa Member*						*Eruption age: 8.5 ± 1.7 ka (INT 2σ: 0.7 ka); n=3*	
231	39.300	175.539	1877.5	0.996	2.11 ± 0.14	0.66 ± 0.06	2.06 ± 0.14	4.91 ± 0.30*
232	39.300	175.539	1873.2	0.991	4.00 ± 0.24	0.74 ± 0.05	3.95 ± 0.24	8.77 ± 0.49
233	39.300	175.539	1872.0	0.994	3.86 ± 0.25	0.93 ± 0.06	3.80 ± 0.25	8.36 ± 0.51
234a	39.300	175.539	1873.4	0.996	3.80 ± 0.24	0.90 ± 0.07	3.73 ± 0.24	
234b	39.300	175.539	1873.4	0.996	3.96 ± 0.27	0.60 ± 0.05	3.92 ± 0.26	
234 mean	39.300	175.539	1873.4	0.996			3.84 ± 0.25	8.44 ± 0.51

https://doi.org/10.5194/egusphere-2024-163
Preprint. Discussion started: 23 January 2024

Table 2: Continued.

Sample	Latitude (S)	Longitude (E)	Elevation (MSL)	Shielding factor	$^{3}He_{tot}$ $\pm1\sigma$ (10^{6}at/g)	$^{4}He_{tot}$ $\pm1\sigma$ (10^{10}at/g)	$^{3}He_{cos}$ $\pm1\sigma$ (10^{6}at/g)	Exposure age $\pm1\sigma$ (ka)
TC	*Turoa Member*					*Eruption age: 13.4 ± 2.6 ka (INT 2σ: 0.7 ka); n=3*		
066	39.301	175.519	1533.2	0.997	4.13 ± 0.20	1.03 ± 0.06	4.06 ± 0.21	11.32 ± 0.52 *
067	39.302	175.519	1533.6	0.997	5.24 ± 0.27	1.14 ± 0.05	5.16 ± 0.26	14.06 ± 0.65
068	39.302	175.519	1533.1	0.997	4.74 ± 0.23	1.09 ± 0.04	4.66 ± 0.23	13.02 ± 0.61
070	39.302	175.519	1528.0	0.997	4.89 ± 0.23	0.82 ± 0.04	4.84 ± 0.23	13.24 ± 0.61
MF	*Makotuku Member*					*Eruption age: 12.5 ± 3.5 ka (INT 2σ: 2.6 ka); n=4*		
061	39.317	175.514	1437.1	0.971	4.92 ± 0.26	1.93 ± 0.07	4.79 ± 0.27	14.23 ± 0.72
063	39.317	175.515	1434.8	0.991	4.00 ± 0.22	2.19 ± 0.09	3.84 ± 0.23	11.35 ± 0.61
064	39.317	175.515	1433.8	0.987	4.08 ± 0.22	1.65 ± 0.07	3.96 ± 0.22	11.73 ± 0.60
065	39.317	175.515	1433.3	0.988	4.47 ± 0.24	1.79 ± 0.08	4.34 ± 0.25	12.71 ± 0.69
NR	*Makotuku Member*					*Eruption age: 42.9 ± 8.6 ka (INT 2σ: 1.7 ka); n=4*		
053	39.338	175.587	1369.8	0.996	16.17 ± 0.67	2.46 ± 0.08	16.05 ± 0.67	46.50 ± 2.10
054	39.338	175.588	1372.9	1.000	15.34 ± 0.63	1.89 ± 0.07	15.19 ± 0.64	43.30 ± 1.74
055	39.338	175.588	1372.7	0.999	14.63 ± 0.62	1.79 ± 0.08	14.49 ± 0.62	41.35 ± 1.74
057	39.338	175.588	1372.6	0.995	14.80 ± 0.62	2.61 ± 0.10	14.63 ± 0.63	42.03 ± 1.61
MA	*Makotuku Member*					*Minimum eruption age: 53.7 ± 17.4 ka (INT 2σ: 14.0 ka); n=2*		
058	39.313	175.612	1594.8	0.996	20.03 ± 0.83	4.82 ± 0.15	19.68 ± 0.84	48.75 ± 2.57
059	39.313	175.612	1593.4	0.998	24.08 ± 1.18	9.56 ± 0.27	23.43 ± 1.19	58.65 ± 2.80
GR	*Mangaehuehu Member*					*Minimum eruption age: 12.7 ± 5.3 ka (INT 2σ: 4.7 ka); n=2*		
023 (Ol)	39.307	175.562	2147.3	0.921	7.61 ± 0.49	1.19 ± 0.13	7.52 ± 0.49	14.42 ± 0.85
024 (Ol)	39.307	175.562	2145.4	0.990	6.19 ± 0.39	1.28 ± 0.07	6.10 ± 0.39	11.07 ± 0.64
025 (Ol)	39.308	175.562	2128.1	0.993	3.61 ± 0.25	1.87 ± 0.10	3.47 ± 0.25	6.76 ± 0.41 *

$^{3}He_{cos}$ values were calculated using Equation 3, with magmatic $^{3}He/^{4}He$ of 7.5 ± 1.5 x 10^{-6}. Individual samples are informed with 1σ for reproducibility using the CREp online calculator. Summary eruption age uncertainties represent 2σ values including production rate errors. Internal (INT) 2σ errors do not include production rate errors. All analysed samples consisted of pure pyroxenes with the exception of the site GR, where analysed crystals were olivines with subordinate pyroxenes. For complete data and corrections, see Table A3. Outliers are marked with * after the calculated exposure age. Two aliquots were measured for samples RTm046 and CTb234, for which we calculated a weighted mean of the $^{3}He_{cos}$ as a sample summary.

5 Discussion

5.1 Consistency with previous age constraints

The new Holocene ^{3}He exposure ages yielded eruption ages with higher precision than $^{40}Ar/^{39}Ar$ dates of Conway et al. (2016) for this time range (Figure 5). Additionally, young (<20 ka) $^{40}Ar/^{39}Ar$ ages of individual samples have normally weak isochrons, as the R values for their linear fits used to calculate crystallization age (released $^{40}Ar/^{36}Ar$ vs $^{39}Ar/^{36}Ar$ in increasing temperature steps) tend to be relatively low (e.g. Harpel et al., 2004; Conway et al., 2016; Preece et al., 2018). Therefore, these ages are very susceptible to the decisions involved in the selection of steps included (or discarded) in the calculation of weighted mean plateau and isochron ages, and our exposure ages based on multiple samples provide more reliable results.

From the four flows sampled in this study with existing $^{40}Ar/^{39}Ar$ dates (Conway et al., 2016), two yielded eruption ages agreeing with the radiometric dates (Delta Corner and Tukino Slopes-b flows), and two outside the 2σ confidence interval of Conway et al. (2016); the Taranaki Falls ($^{3}He/_{cos}$: 14.6 ± 2.9 ka; $^{40}Ar/^{39}Ar$: 8.8 ± 2.8 ka) and the Lava Cascade ($^{3}He/_{cos}$: 11.4 ± 2.3 ka; $^{40}Ar/^{39}Ar$: 0.8 ± 5.6 ka) flows. Based on the good clustering of our results (Table 2), we suggest that our $^{3}He_{cos}$ eruption age better represents the true eruption age of the Taranaki Falls flow. Additionally, our eruption age would explain the rootless nature of the flow (Townsend et al., 2017), as it precedes the flank collapse event that affected the northern summit area of Ruapehu at *ca* 10.5 ka (Eaves et al., 2015). The imprecise nature of the radiometric age of the Lava Cascade flow and its weak

https://doi.org/10.5194/egusphere-2024-163
Preprint. Discussion started: 23 January 2024

isochron, together with the good agreement between our LC samples and the eruption ages we obtained for the Mangatoetoenui flows, leads us to conclude that our eruption age for the Lava Cascade flow is more robust than the date provided by Conway et al. (2016).

Our results show, in general, good agreement with lava flow eruption ages refined by Greve et al. (2016) at Ruapehu Figure 5. The only exception is the Taranaki Falls flow, which refinement by Greve et al. is based on the $^{40}Ar/^{39}Ar$ date of Conway et al. (2016), thus it intrinsically agrees with this age and not with our results. Our $^{3}He_{cos}$ eruption ages for the Delta Corner (7.8 ± 1.5 ka; INT 2σ 0.6 ka), Bruce Road (8.0 ± 2.1 ka; INT 2σ 1.5 ka) and Saddle Cone (9.8 ± 2.0 ka; INT 2σ 0.7 ka) flows match the respective age ranges of 8200–7900, 8800–8500 and 9850–8650 BP provided by Greve et al. (2016). Moreover, these results suggest that it is unlikely that P_3 errors have a significant impact on the accuracy of the eruption ages from this work, which is also supported by the good agreement of the local $^{3}He_{cos}$ production rate calibration test by Eaves et al. (2015) with the world wide mean production rate used in this study.

Most of the flows dated in this study lack previous age constraints beyond estimations based on geochemical similarity and geographical proximity to lavas with $^{40}Ar/^{39}Ar$ dates. The eruption ages obtained for about half of these flows do not agree with these correlations (Figure 5). Five of them (MN, MS, CTb, MF and GR flows) yielded ages younger than any of the dates informed for the units they were correlated to (i.e., Turoa, Makotuku and Mangaehuehu members). This can be explained by to a sampling bias of Conway et al. (2016) towards older flows, more likely to have exposed their slowly-cooled flow interiors (suitable for $^{40}Ar/^{39}Ar$ dating) due to their longer periods exposed to erosive processes and the presence of collapsed thick margins in the case of previously ice-impounded flows (Conway et al., 2015). PR and MA deposits are relatively isolated (Figure 4a, b), so the previous geochemical correlations are weaker. The age previously assigned to the PR deposits (Table 1) was, unlike any other lava in this study, based on a correlation with a pyroclastic unit, adding another layer of uncertainty. Our results represent the first dates for lavas at the the PR and MA sites and indicate older eruption ages than suggested by geochemical correlations.

The TFt site is located at a lower elevation (*ca* 1515 m asl) and was expected to yield equal or older eruption ages, compared to the other flows from the Mangatoetoenui Flows unit. Our results for the three TFt samples (7.7, 10.7 and 7.3 ka) do not meet this stratigraphic constraint, and the lack of additional samples hindered our ability to obtain a robust eruption age. Considering a combined minimum eruption age of 8.6 ± 4.6 ka, the ages of the other flows from the Mangatoetoenui flows, and their stratigraphic position, our best estimate for the Tukino Flats flow is 12–10 ka.

Eruption ages obtained for the Rangataua medial and proximal flows (15.7 ± 3.0 and 13.5 ± 2.6 ka, respectively) do not agree with a 12–10 ka constraint suggested by Price et al. (2012, based on unpublished data) based on tephra stratigraphy. However, tephra correlation on Ruapehu is complex due to the large number of pyroclastic units emplaced at 20–11 ka and their broad geochemical ranges (Pardo et al., 2012). Detailed studies (Donoghue et al., 2007) attempted to systematize tephra correlation in this area without success, indicating that the andesitic tephras are highly heterogeneous, displaying wide compositional fluctuations during short time intervals. The other existing constraint for the Rangataua flows was given by a right lateral moraine of the Mangaehuehu Valley dated at 11–14 ka by Eaves et al. (2019), which was thought to correspond in age to the left lateral moraine overlain by the RTm flow (Figure 4d). Our eruption age of 15.7 ± 0.8 ka (INT 2σ, P_3 errors not considered as the moraines were dated using $^{3}He_{cos}$) suggests that the moraine underlying the Rangataua flows is older than the dated right lateral moraine, rather than its equivalent.

5.2 Inconsistency with previous classification of units

Most of the eruption ages measured in this study are consistent with the age and geochemical ranges of the units to which they were assigned by Townsend et al. (2017). Here, we discuss the results we obtained which do not agree with the existing classification.

- Donoghue et al. (1999) linked the Pinnacle Ridge spatter-fed lava with the Taurewa pyroclastic unit (*ca* 10 ka) based on geochemistry and the concentric nature of the Taurewa deposits' isopachs around the location of PR. Our results suggest that the Pinnacle Ridge deposit was emplaced at 20.2 ± 3.9 ka, during the LGM and *ca* 10 ka prior to the Taurewa eruptive event. Our eruption age for Pinnacle Ridge further suggests that this unit should be included as part of the Mangawhero Formation (50–15 ka) instead of the Whakapapa Formation (<15 ka), which is consistent with the lack of preservation of a proximal vent, likely associated to a significant erosive period and the retreat of large ice masses.

- MF samples were taken from a large flow considered to be part of the Makotuku Member of the Mangawhero Formation (*ca* 24–16 ka, Table 1) based on its geochemistry. Our results show that this lava flow —which reached the Makotuku valley bottom (Figure 4d)— was erupted at 12.5 ± 3.5 ka, which suggests that, based on age criteria, it could be classified as part of the Whakapapa Formation (<15 ka).

- Our NR site was mapped as part of the Makotuku Member, on an area dominated by outcrops of Mangaehuehu lavas (Figure 4d). Our eruption age of 42.9 ± 8.6 ka for this site, together with NR's samples geochemical similarity to Mangaehuehu lavas (47–40 ka; Conway et al., 2016, see Table 1), suggests that the sampled outcrop is part of the Mangaehuehu Member.

- The outcrop we collected the MA samples from has, due to its geochemical similarity, been considered part of the Makotuku Member. Two exposure ages indicate that the Makahikatoa flow was emplaced at, or prior to, 50 ka, suggesting that it was formed during the first eruptive stages of the Mangawhero or in the late stages of the Waihianoa Formation (see Table 1), with a geochemical signature common in lavas emplaced at 24–16 ka.

- Exposure ages of GR samples (previously mapped as part of the Mangaehuehu Member) suggest that this lava was emplaced during the last 15 ka, which is inconsistent with it being part of the Mangawhero Formation. However, its geochemistry differentiate this outcrop from the rest of the Whakapapa lavas (Conway et al., 2016), thus it is likely part of a new member within the Whakapapa Formation.

https://doi.org/10.5194/egusphere-2024-163
Preprint. Discussion started: 23 January 2024

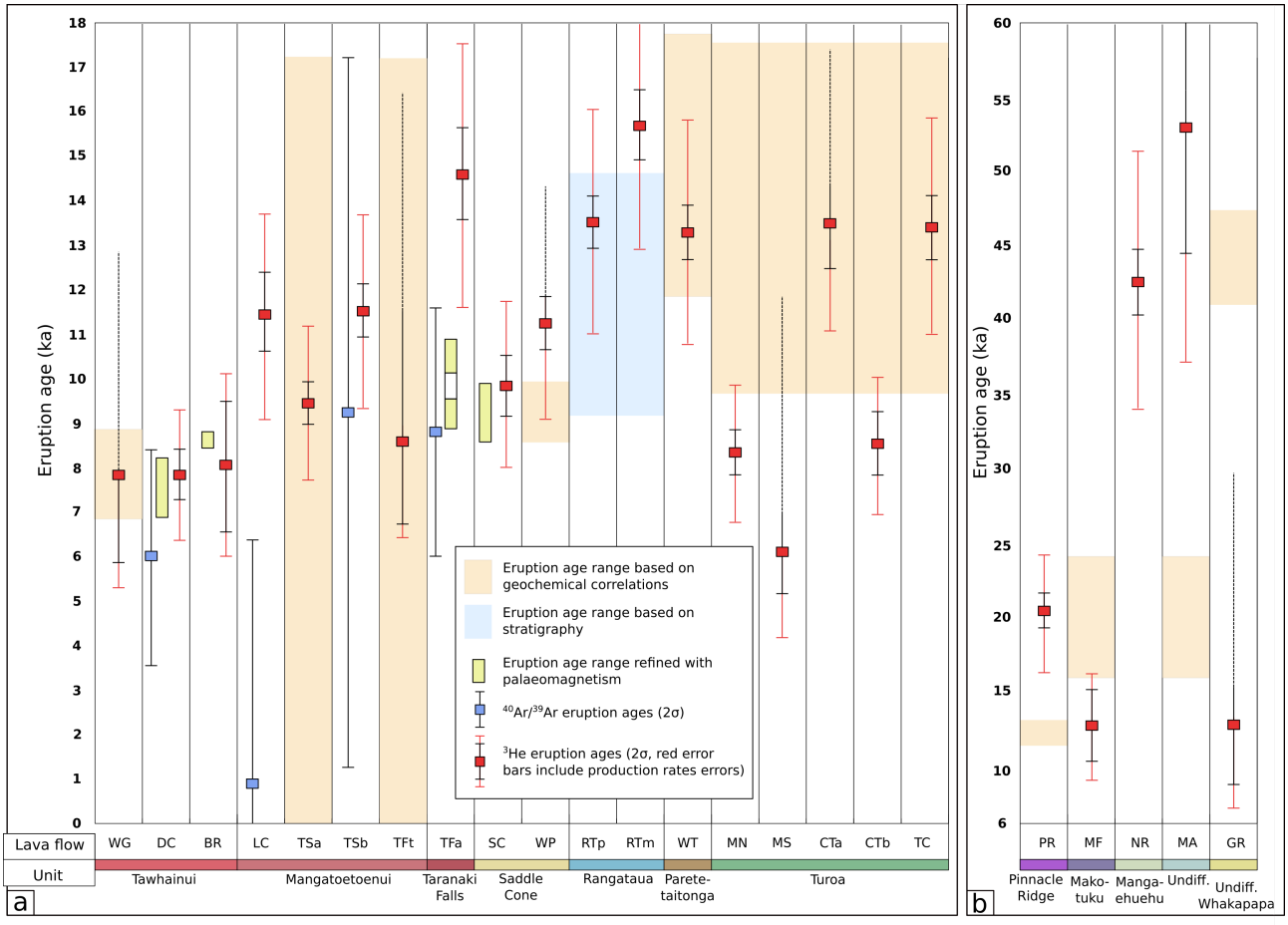

Figure 5. Comparison between eruption ages obtain in this study and previous chronological constraints of the sampled flows. Unit colours correspond to the colours on Figure 1. a) Lavas <20 ka. b) Lava flows that are —or were thought to be— older than 20 ka.

- The results we obtained for flows from the Turoa Member indicate that lava was emplaced on Ruapehu's western flanks at *ca* 15–12 ka (Turoa Cascades and Central Turoa-a flows, as well as Conway et al., 2016) and, after a hiatus of *ca* 4 ka, again at around 8 ka (Mangaturuturu North and Central Turoa-b flows). Thus, we suggest the extension of the younger limit of the Turoa Member to 8 ka.

- Similarly to the Turoa Member, the obtained eruption ages redefine the age limits of the Rangataua Member (17–12 ka), Saddle Cone Member (12–8.5 ka), Taranaki Falls flow (16–13 ka) and Mangatoetoenui flows (12–9 ka).

5.3 Postglacial effusive activity of Ruapehu

Our $^{3}He_{cos}$ based eruption ages provide new insights on the postglacial effusive chronology of Ruapehu, allowing periods of enhanced effusive activity since the LGM to be identified (17–12 ka, Figure 6a and b; and 9–7.5 ka, Figure 6e), during which lava emplacement on different areas of the volcano occurred nearly simultaneously.

Our results show that, during the last glacial termination (*ca* 17–14 ka; Figure 6a), effusive activity affected the southern (Rangataua medial and, likely, the distal Rangataua flows) and northern (Taranaki Falls flow) slopes of Ruapehu, suggesting that the volcano's southern and northern vents were active during this period. Radiometric dates published by Conway et al. (2016, see Table 1) suggest that, during this period, lava flows were also emplaced on Ruapehu's western (15.1 ± 2.4 ka, Turoa Member) and northwestern (14.8 ± 3.0 ka, Paretetaitonga Member) flanks. This period of generalized activity across Ruapehu continued until *ca* 12 ka (Figure 6b), with increasing intensity on the western and decreasing intensity on the southern flanks. Eruption ages of the Whakapapaiti (13.3 ± 0.6 ka), Turoa Cascades (13.4 ± 0.7 ka) and Rangataua proximal (13.5 ± 0.6 ka) flows

https://doi.org/10.5194/egusphere-2024-163
Preprint. Discussion started: 23 January 2024

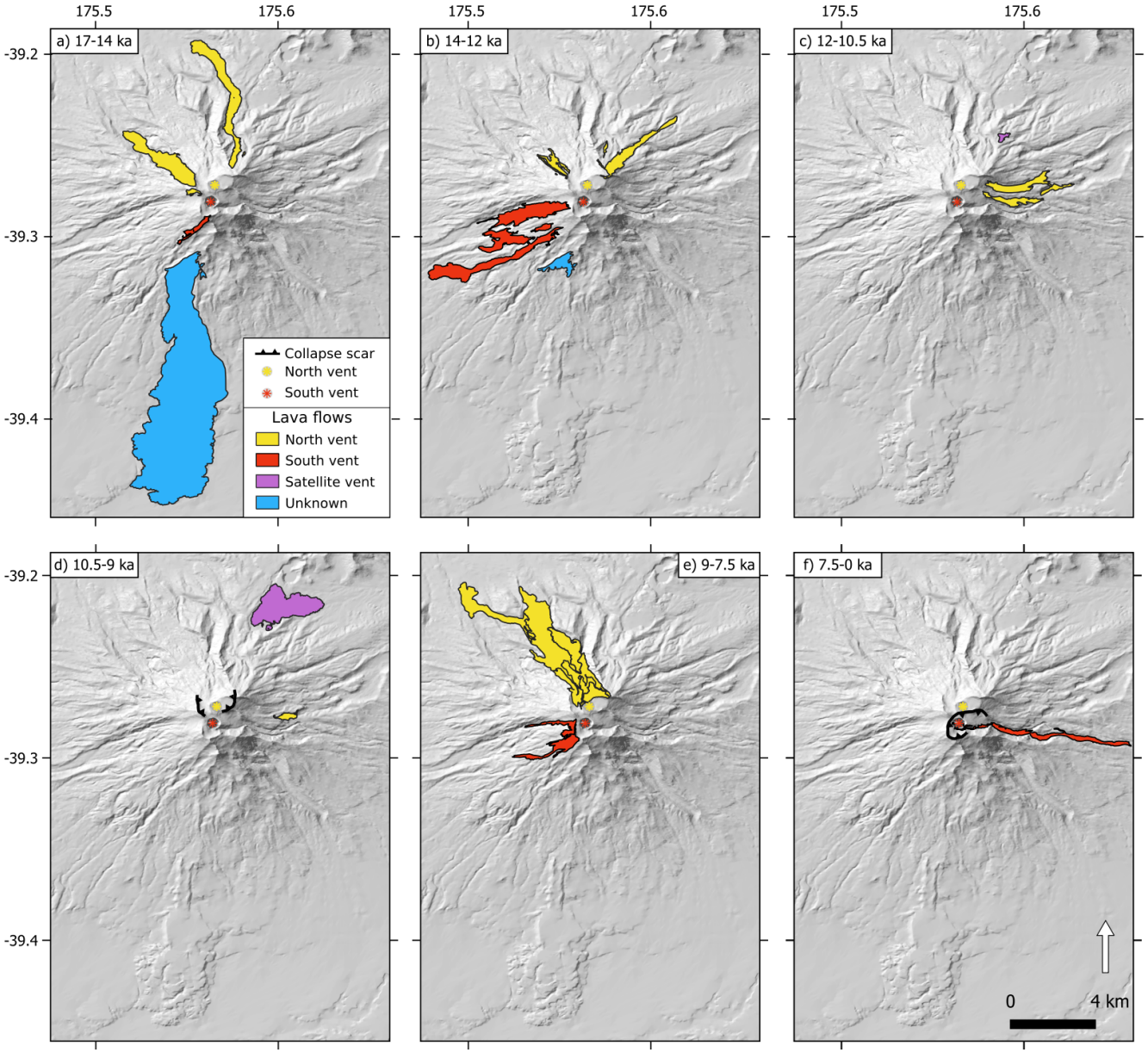

Figure 6. Lava flows emplaced at Ruapehu through time after the LGM. Collapse scars corresponds to flank collapse episodes at 10.4–10.6 cal ka BP (Murimotu debris avalanche; Eaves et al., 2015) and at ∼4.6 ka, (Mangaio Formation; Donoghue, 1991; Donoghue and Neall, 2001).

are nearly identical, indicating that lava emplacement occurred nearly simultaneously on different flanks of the volcanic edifice. In the early Holocene (i.e. 12–10.5 ka, Figure 6c), activity was focused on the east and northeast of the volcano, generating the first lavas of the Mangatoetoenui flows, as well as lavas emerging from satellite vents (Waihohonu Plateau flow). After a flank collapse that affected part of the northern edifice at ∼10.5 ka (Eaves et al., 2015), lava flows continued to be emplaced on the eastern flanks from the

https://doi.org/10.5194/egusphere-2024-163
Preprint. Discussion started: 23 January 2024

northern vent and erupting from satellite vents on the northeast in short time lapses (<2 kyr), generating the large Saddle Cone flow (Figure 6d). The rate of lava production between 9 and 7.5 ka (Figure 6e) was likely to have been the highest in the last 20 ka at Ruapehu. Our results suggest that, during this time, most of the flows forming the Tawhainui sequence on north Ruapehu were emplaced from the northern vent, filling a topographic low left by the flank collapse. Similarly in time, the last lavas of the Turoa Member (Mangaturuturu North and, Central Turoa-b flows) were being erupted from the southern vent and flowed to the west of the edifice. Effusive activity then declined, and after another episode of flank collapse that modified the topography surrounding the summit southern vent, lava flow emplacement was confined to the current outlet of Ruapehu's crater lake and flowed to the east (Whangaehu valley, Figure 6f) at 2400–2050 BP (Greve et al., 2016).

5.4 Applicability of cosmogenic ^{3}He dating on stratovolcanoes

The ability to obtain robust eruption ages of prehistoric lava flows using surface exposure dating depends on the preservation of the lavas' original surfaces, as well as a limited to no rock, vegetation, soil, tephra, ice or snow cover that could have shielded the influx of cosmic particles. In temperate climates, suitable sites will lie at elevations between the vegetation limit and where cryogenic processes begin to dominate (*ca* 2150–1300 m asl at Ruapehu). In dynamic environments such as stratovolcanoes, original surfaces are more likely to be preserved on younger lava flows, which have had a relatively limited time exposed to erosive and/or depositional processes. In addition, flow interiors with crystalline groundmass necessary for ^{40}Ar/^{39}Ar or K/Ar dating are less likely to be exposed in young lava flows for the same reason.

Sources of uncertainties of ^{3}He$_{cos}$ dating comprise analytical errors, corrections for non-cosmogenic ^{3}He, and P_3 errors. The relative magnitude of analytical errors depends on blank levels achieved at the laboratory and the concentration of measured ^{3}He, which increases with exposure duration and P_3 (higher at higher elevations). Uncertainties related to non-cosmogenic ^{3}He corrections depend on magmatic He values and local magmatic ^{3}He/^{4}He ratio; and ^{3}He$_{nuc}$ and ^{4}He$_{rad}$ corrections, which vary with the rock's and minerals' geochemistry, respectively, P_3, and mineral closure age. These uncertainties can be as high as 100% in the worst-case scenarios (Blard, 2021) and are larger for rocks: at lower elevations; with high (e.g. 10^{11}) ^{4}He$_{mag}$; with smaller closure age/exposure age ratios (not applicable for dating lava flows); and with high concentration of radioactive elements and Li (normally higher on more evolved rocks). In most cases, however, P_3 uncertainty has the largest contribution on exposure age errors when using ^{3}He$_{cos}$ dating, imparting an uncertainty of *ca* 10% to all calculated ages. Thus, more high-quality calibration sites are required to reduce these uncertainties and improve the quality of ^{3}He-based exposure ages.

Considering these sources of uncertainties, the resolution of ^{3}He$_{cos}$-based eruption ages can be higher than ^{40}Ar/^{39}Ar or K/Ar for young intermediate and basic lavas (e.g. Figure 5). The older the lava flow, however, the higher its crystallization age resolution based on radiometric methods will be, while if dated using TCNs its exposure age uncertainty would increase due to the influence of cosmogenic nuclide production rate errors. Consequently, cosmogenic nuclides exposure dating has the potential to yield better results compared to ^{40}Ar/^{39}Ar or K/Ar when dating <14 ka lava flows, and offers a valid alternative to date older lavas when no radiometric dating method can be applied (e.g. the site NR from this study, which ages match with higher-precision ^{40}Ar/^{39}Ar dates of geochemically similar lavas).

6 Conclusions

We analysed pyroxene- and olivine-hosted ^{3}He$_{cos}$ on 80 samples from 23 lava flows of Ruapehu volcano, New Zealand, and obtained 16 eruption ages (between 7.8 $\pm$ 0.6 and 42.9 $\pm$ 1.7 ka; analytic 2σ) and seven minimum eruption ages, refining the chronology of lava flow emplacement at Ruapehu in the last 20 kyr. Our analyses show good agreement with previous high-resolution age constraints, suggesting that ^{3}He$_{cos}$ production rate errors do not affect the accuracy of our eruption ages.

Our results show effusive activity at Ruapehu occurred nearly simultaneously from different vents during the last 17 ka, affecting various sectors of the volcanic edifice over short time intervals. Based on our observations, we propose that the number of effusive eruptions and the volume involved peaked at 17–12 and 9–7.5 ka.

We have demonstrated how cosmogenic nuclides exposure dating can provide greater detail on the recent effusive chronology of statovolcanoes, filling the gap left by the low resolution and challenges in adequate samples acquisition of radiometric dating methods applied on young lava flows.

Data availability. All used data is available in the supplementary file S1 and appendix table A2.

https://doi.org/10.5194/egusphere-2024-163
Preprint. Discussion started: 23 January 2024

Abbreviation	Lava Flow Name	Area
BR	Bruce Road	North
CTa	Central Turoa-a	West
CTb	Central Turoa-b	West
DC	Delta Corner	North
GR	Girdlestone Ridge	South
LC	Lava Cascade	East
MA	Makahikatoa	Southeast
MF	Makotuku Flat	West
MN	Mangaturuturu North	West
MS	Mangaturuturu South	West
NR	Ngā Rimutāmaka	South
PR	Pinnacle Ridge	North
RTm	Rangataua medial	South
RTp	Rangataua proximal	South
SC	Saddle Cone	Northeast
SCw	Saddle Cone - western lobe	Northeast
SCe	Saddle Cone - eastern lobe	Northeast
TC	Turoa Cascades	West
TFa	Taranaki Falls	North
TFt	Tukino Flats	East
TSa	Tukino Slopes-a	East
TSb	Tukino Slopes-b	East
WG	Whakapapa Glacier	North
WP	Waihohonu Plateau	Northeast
WT	Whakapapaiti	Northwest

Table A1. Abbreviations list, used for sampling sites and samples.

Table A2. Normalized major and trace elements of bulk rock and analysed crystals for each sampled lava flow.

Bulk rock	normalized wt.%												ppm							
Site	**SiO_2**	**Al_2O_3**	**Fe_2O_3**	**MnO**	**MgO**	**CaO**	**Na_2O**	**K_2O**	**TiO_2**	**P_2O_5**	**LOI**	**Maj_{tot}**	**Li**	**B**	**Cr**	**Co**	**Ni**	**Gd**	**Sm**	**U**	**Th**
DC	57.01	15.88	8.23	0.13	5.37	7.42	3.14	1.40	0.68	0.18	0.56	99.26	17.9	20.0	85.19	26.68	45.59	2.69	2.75	1.08	4.04
BR	55.80	16.49	7.69	0.12	4.74	6.38	3.11	1.55	0.68	0.14	3.31	100.23	20.4	22.8	101.82	23.64	40.78	2.79	2.83	1.30	4.91
WG	54.87	16.02	9.25	0.13	5.34	6.59	2.92	1.41	0.72	0.14	2.62	99.46	17.6	20.1	91.32	26.95	45.80	2.75	2.75	1.13	4.36
LC	52.61	18.94	8.79	0.13	4.21	5.18	2.65	1.52	0.78	0.15	5.04	99.79	19.6	20.5	64.56	21.82	20.55	2.87	2.84	1.46	5.22
TSa	53.97	17.20	8.91	0.13	4.36	6.51	2.81	1.41	0.79	0.16	3.76	99.52	16.3	19.6	45.17	22.39	14.11	2.79	2.81	1.19	4.79
TSb	52.75	18.33	8.68	0.13	4.62	5.87	2.64	1.42	0.77	0.14	4.65	100.47	19.0	20.0	85.21	24.29	24.85	2.79	2.76	1.42	5.03
TFt	55.98	17.28	8.40	0.13	4.26	6.59	2.94	1.42	0.75	0.13	2.11	100.05	17.2	21.2	56.97	21.95	18.92	2.61	2.57	1.23	4.61
TFa	57.17	16.80	7.81	0.12	4.09	6.88	3.15	1.52	0.72	0.13	1.61	100.25	16.8	22.3	60.99	20.34	19.91	2.91	2.96	1.34	5.09
SC	56.76	16.48	7.88	0.12	4.64	7.02	3.07	1.52	0.72	0.15	1.63	99.87	21.3	21.7	86.23	23.75	31.36	2.77	2.81	1.32	4.92
WP	55.42	16.60	8.13	0.12	4.87	6.58	2.77	1.31	0.70	0.13	3.37	100.04	18.8	20.3	95.47	24.80	36.95	2.72	2.60	1.18	4.49
PR	58.59	16.12	6.78	0.10	4.42	5.69	3.04	1.79	0.65	0.14	2.68	100.29	22.5	21.9	183.67	20.39	53.61	2.57	2.50	1.45	5.50
RTp	56.56	17.39	7.60	0.12	3.37	5.35	3.15	1.74	0.75	0.15	3.84	99.83	19.2	23.9	36.93	16.88	12.67	3.00	3.11	1.49	5.91
RTm	56.64	16.82	7.67	0.12	3.57	5.72	3.15	1.69	0.75	0.21	3.67	99.53	18.6	23.4	40.90	17.75	13.20	3.15	3.17	1.53	6.03
WT	55.32	17.34	8.29	0.12	4.19	5.79	2.85	1.52	0.76	0.14	3.69	100.24	20.3	20.9	57.45	20.84	18.59	2.76	2.80	1.32	5.40
MN	53.66	17.72	8.07	0.12	5.01	6.09	2.93	1.47	0.66	0.13	4.14	100.44	19.2	22.5	93.87	25.17	47.08	2.42	2.41	1.34	4.86
MS	55.58	15.71	9.54	0.13	4.51	6.18	2.87	1.49	0.84	0.13	3.01	100.20	13.8	19.2	54.80	23.51	17.53	2.45	2.45	0.94	4.99
CTa	56.67	16.49	8.12	0.12	4.36	6.49	3.01	1.50	0.72	0.15	2.37	99.64	20.2	21.8	88.79	22.15	29.15	2.75	2.80	1.35	5.02
CTb	56.01	16.78	8.32	0.12	4.60	7.12	3.01	1.39	0.74	0.13	1.77	99.29	19.3	20.8	89.86	23.46	27.88	2.72	2.75	1.20	4.51
TC	56.18	16.49	8.44	0.13	4.60	7.03	3.06	1.48	0.78	0.14	1.66	99.90	17.3	20.0	71.52	22.48	18.63	2.96	2.95	1.22	4.71
MF	58.67	16.98	6.52	0.093	2.96	5.91	3.50	1.87	0.84	0.16	2.50	100.13	26.8	27.3	49.22	16.60	18.75	2.96	3.13	1.63	6.12
NR	57.92	14.71	6.81	0.11	6.24	5.96	2.96	1.85	0.73	0.19	2.53	99.77	29.7	23.4	308.14	25.08	109.34	3.14	3.25	1.74	6.50
MA	58.73	17.28	6.77	0.10	3.09	5.26	3.29	1.55	0.68	0.13	3.12	99.82	21.0	24.4	34.02	17.42	14.05	2.77	2.85	1.31	5.00
GR	55.76	15.21	7.40	0.12	6.09	6.77	2.80	1.35	0.66	0.14	3.71	100.13	20.4	20.7	215.77	26.79	73.65	2.71	2.78	1.14	4.50
Crystals																					
DC	52.11	1.58	20.53	0.41	22.11	4.08	0.09	<DL	0.31	<DL	-1.20	99.63	<2	10.7	285.89	98.63	187.40	1.07	0.78	0.01	0.040
BR	51.76	1.97	18.03	0.36	19.70	8.31	0.20	0.04	0.39	<DL	-0.76	99.55	<2	8.59	398.47	85.29	172.81	2.37	1.97	0.04	0.144
WG	51.71	1.61	20.15	0.39	21.71	4.76	0.10	<DL	0.34	<DL	-0.77	99.85	<2	12.8	371.23	92.22	182.44	1.38	1.08	0.01	0.048
LC	51.54	1.59	20.41	0.43	20.50	5.74	0.12	<DL	0.39	<DL	-0.71	99.32	<2	10.7	337.72	85.76	129.55	1.97	1.60	0.02	0.056
TSa	49.38	1.51	24.99	0.44	21.19	2.14	0.05	<DL	0.86	<DL	-0.57	99.83	<2	7.35	404.65	98.37	143.62	0.65	0.44	0.02	0.052
TSb	51.60	1.52	21.23	0.45	21.34	4.16	0.08	<DL	0.37	<DL	-0.76	100.32	<2	10.9	277.49	88.05	117.96	1.39	1.08	0.01	0.050
TFt	51.18	1.53	21.60	0.45	20.94	4.64	0.09	<DL	0.49	<DL	-0.90	99.54	<2	16.7	279.53	88.18	120.06	1.59	1.27	0.01	0.047
TFa	51.27	1.51	20.55	0.42	20.94	5.09	0.10	<DL	0.40	<DL	-0.28	99.10	<2	11.0	367.38	85.09	130.22	1.65	1.35	0.02	0.062
SC	51.41	1.91	19.70	0.39	19.54	7.18	0.18	0.04	0.42	<DL	-0.78	100.00	<2	9.17	394.61	80.89	127.03	2.56	2.07	0.05	0.185
WP	52.19	2.37	16.91	0.33	19.95	8.16	0.28	0.10	0.38	<DL	-0.67	99.86	<2	10.2	645.87	77.50	164.79	2.21	1.80	0.10	0.358
PR	51.05	2.01	20.06	0.39	20.02	6.31	0.13	<DL	0.41	<DL	-0.39	99.57	<2	31.0	632.12	83.14	163.52	1.94	1.54	0.03	0.141
RTp	51.08	1.50	22.65	0.43	21.53	3.04	0.07	<DL	0.49	<DL	-0.80	100.29	<2	5.71	405.44	91.30	153.24	1.06	0.80	0.01	0.049
RTm	51.38	1.46	23.10	0.44	21.71	2.91	0.06	<DL	0.47	<DL	-1.53	99.84	<2	7.48	321.50	91.05	135.00	1.07	0.82	0.01	0.045
WT	47.28	1.59	26.88	0.43	20.27	2.90	0.06	<DL	1.41	<DL	-0.82	99.76	<2	10.7	465.85	96.87	142.07	0.89	0.68	0.03	0.069
MN	52.02	1.51	21.69	0.43	22.68	2.47	0.06	<DL	0.31	<DL	-1.18	99.37	<2	13.4	269.95	102.76	196.34	0.66	0.46	0.01	0.040
MS	51.76	1.62	20.40	0.42	21.30	5.00	0.10	<DL	0.38	<DL	-0.97	99.36	<2	23.6	374.34	88.31	122.86	1.52	1.20	0.01	0.046
CTa	51.45	1.64	20.05	0.41	20.42	5.92	0.13	<DL	0.38	<DL	-0.40	99.89	<2	9.23	409.65	84.51	143.50	2.11	1.72	0.03	0.098
CTb	51.08	1.63	20.86	0.41	20.43	5.87	0.12	<DL	0.62	<DL	-1.03	99.35	<2	10.8	410.51	84.63	144.39	2.03	1.67	0.02	0.065
TC	51.56	1.62	20.37	0.41	21.10	5.02	0.10	<DL	0.35	<DL	-0.53	100.21	<2	8.01	391.62	88.11	124.68	1.51	1.19	0.01	0.046
MF	50.94	1.66	22.07	0.39	21.93	3.35	0.07	<DL	0.82	<DL	-1.22	99.65	<2	13.6	475.60	95.40	181.14	0.94	0.73	0.02	0.058
NR	52.64	1.95	16.10	0.28	22.62	6.82	0.15	<DL	0.35	<DL	-0.90	99.71	<2	11.7	1184.21	83.92	352.04	1.56	1.27	0.02	0.042
MA	49.70	2.03	22.77	0.39	21.09	3.88	0.08	<DL	0.89	<DL	-0.83	99.44	<2	17.7	332.48	92.02	106.83	0.88	0.64	0.02	0.081
GR	54.07	1.52	13.92	0.27	27.48	2.89	0.05	<DL	0.19	<DL	-0.39	99.30	<5	6.22	1649.09	87.13	360.96	0.36	0.26	<DL	0.022

Detection limits (DL) are 0.03 wt.% for K_2O; 0.10 wt.% for P_2O_5; 2 ppm for B; and 0.01 ppm for U.

Table A3: Sample data used to compute exposure ages.

Sample	Latitude (S)	Longitude (E)	Elevation (MSL)	Surface dip (°)	Dip direction (°)	Shielding factor	Density (g/cm^3)	Thickness (cm)	P_{nuc} (10^2 at/g/yr)	Closure age (Ma)	He_{nuc} (at)	P_3 (at/g/yr)	P_4 (10^5 at/g/yr)	R factor
SC 001	39.214	175.601	1439.0	-	-	0.998	1.89	3.61	406	0.010	406	231.22	3.13	0.9932
SC 002	39.214	175.601	1439.3	-	-	0.998	2.01	3.17				245.83		0.9932
SC 003	39.215	175.600	1443.3	-	-	0.998	2.01	2.35				245.86		0.9932
WP 007	39.248	175.588	1911.7	10	190	0.996	2.13	3.25	414	0.010	415	487.90	6.08	0.9906
WP 008	39.248	175.588	1912.1	18	30	0.995	2.06	3.02				487.90		0.9906
BR 014	39.220	175.541	1360.0	-	-	0.999	2.15	2.73	565	0.010	565	317.93	0.75	0.9982
BR 016	39.220	175.538	1359.2	28	55	0.981	2.32	2.63				320.37		0.9982
BR 017	39.219	175.541	1332.6	-	-	0.998	2.25	2.71				313.04		0.9982
BR 018	39.219	175.541	1332.4	-	-	0.998	2.15	4.33				317.93		0.9982
GR 023	39.307	175.562	2147.2	45	180	0.921	2.24	4.46	254	0.020	508	584.50	0.44	0.9994
GR 024	39.307	175.562	2145.4	-	-	0.990	2.18	4.61				574.72		0.9994
GR 025	39.308	175.561	2128.1	-	-	0.993	2.80	4.72				539.25		0.9994
RT 027	39.314	175.551	1831.4	-	-	0.997	1.84*	5.48	296	0.015	444	468.33	0.74	0.9988
RT 028	39.314	175.551	1833.1	-	-	0.996	1.79	5.33				467.11		0.9988
RT 029	39.314	175.551	1832.9	-	-	0.996	1.84*	5.33				469.56		0.9988
RT 030	39.314	175.551	1816.4	20	230	0.988	1.89	5.05				465.89		0.9988
RT 045	39.323	175.552	1585.9	20	80	0.991	2.80	4.23	401	0.015	601	399.86	0.75	0.9986
RT 046	39.325	175.551	1567.6	29	145	0.979	2.07	3.61				393.74		0.9986
RT 047	39.325	175.550	1567.4	-	-	0.997	2.27	3.03				392.52		0.9986
RT 048	39.325	175.550	1567.3	-	-	0.997	2.19	3.38				374.18		0.9985
NR 053	39.338	175.587	1369.8	15	3	0.996	2.39	4.83	654	0.045	2944	359.50	1.01	0.9979
NR 054	39.338	175.588	1372.9	-	-	1.000	2.06	4.21				360.73		0.9979
NR 055	39.338	175.588	1372.5	-	-	0.999	2.15	3.22				358.28		0.9979
NR 057	39.338	175.588	1372.6	-	-	0.995	2.47	3.50				359.50		0.9979
MA 058	39.313	175.612	1570.7	14	190	0.996	2.45	2.88	818	0.050	4089	414.53	1.29	0.9977
MA 059	39.313	175.612	1569.3	-	-	0.998	2.21	3.19				408.42		0.9976
MF 061	39.317	175.514	1437.0	-	-	0.971	2.15	3.03	729	0.013	948	353.39	1.14	0.9975
MF 063	39.317	175.515	1434.8	-	-	0.991	1.81	3.77				348.50		0.9975
MF 064	39.317	175.515	1433.8	-	-	0.987	1.95	3.57				349.72		0.9975
MF 065	39.317	175.515	1433.3	11	180	0.988	1.80	2.60				350.94		0.9975
TC 066	39.301	175.519	1533.2	-	-	0.997	2.17	6.23	292	0.013	380	375.40	7.59	0.9985
TC 067	39.302	175.519	1533.6	-	-	0.997	2.11	4.46				379.07		0.9985
TC 068	39.301	175.519	1533.1	-	-	0.997	2.15	7.41				377.85		0.9985
TC 070	39.301	175.519	1528.0	-	-	0.997	1.99	4.33				376.62		0.9985
WT 073	39.257	175.543	1892.4	20	260	0.987	2.09	3.53	493	0.013	641	468.33	0.77	0.9984
WT 074	39.257	175.543	1892.1	-	-	0.988	2.22	3.75				471.99		0.9984
WT 075	39.257	175.543	1891.2	-	-	0.997	2.18	3.25				471.99		0.9984
PR 083	39.237	175.567	1730.7	16	310	0.979	2.28	3.54	1557	0.020	3115	453.66	2.11	0.9965
PR 084	39.239	175.569	1860.9	24	180	0.988	2.18	4.66				492.79		0.9968
PR 085	39.238	175.569	1857.9	16	330	0.997	2.12	4.25				497.68		0.9968
TFa 088	39.207	175.567	1308.2	-	-	0.999	2.39	3.75	513	0.015	769	321.60	1.17	0.9973
TFa 090	39.206	175.567	1290.4	16	90	0.996	2.31	5.00				316.71		0.9972
TFa 091	39.206	175.566	1288.2	-	-	0.999	2.23	4.20				317.93		0.9972
SC 093	39.212	175.614	1308.2	17	40	0.993	2.30	2.59	537	0.010	537	313.04	3.71	0.9911
TSa 205	39.276	175.602	1905.0	-	-	0.983	2.12	5.58	305	0.010	305	476.89	1.05	0.9983
TSa 206	39.276	175.602	1905.9	-	-	0.997	2.21	4.84				480.56		0.9984
TSa 207	39.276	175.602	1905.5	-	-	0.997	2.37	4.16				481.78		0.9984

Table A3: Continued.

Sample	Latitude (S)	Longitude (E)	Elevation (MSL)	Surface dip (°)	Dip direction (°)	Shielding factor	Density (g/cm^3)	Thickness (cm)	P_{nuc} (at/g/yr)	Closure age (Ma)	He_{nuc} (at/g)	P_3 (at/g/yr)	P_4 (10^5 at/g/yr)	R factor
TSb 209	39.282	175.599	1932.5	-	-	0.997	2.20*	2.42	506	0.010	506	494.01	0.75	0.9989
TSb 210	39.282	175.599	1935.0	17	90	0.989	2.14	2.90				500.13		0.9988
TSb 211	39.282	175.599	1929.2	20	110	0.993	2.26	3.68				497.68		0.9988
TFt 212	39.273	175.626	1521.2	-	-	0.994	2.07	5.85	703	0.010	703	359.50	0.76	0.9984
TFt 213	39.273	175.626	1522.0	10	40	0.998	2.14	6.48				369.29		0.9985
TFt 214	39.272	175.627	1506.4	-	-	0.988	2.23	6.45				353.39		0.9984
MN 217	39.283	175.532	1815.9	-	-	0.993	2.11	2.62	623	0.008	498	446.32	0.65	0.9989
MN 218	39.283	175.532	1813.9	13	220	0.993	2.24	5.19				448.77		0.9989
MN 219	39.283	175.532	1812.1	-	-	0.993	2.22	3.99				425.53		0.9988
MN 220	39.283	175.532	1817.5	-	-	0.993	2.06	3.22				449.99		0.9989
MN 221	39.283	175.533	1822.8	-	-	0.993	2.20	4.03				446.32		0.9989
MS 222	39.284	175.530	1750.6	36	170	0.955	2.23	4.97	901	0.010	901	414.53	0.76	0.9986
MS 223	39.284	175.531	1751.4	-	-	0.992	2.41	4.01				412.08		0.9986
MS 224	39.284	175.530	1750.9	-	-	0.992	2.33	4.10				401.08		0.9986
CTa 229	39.296	175.539	1924.0	7	300	0.996	1.96	3.15	415	0.015	623	498.90	1.81	0.9972
CTa 230	39.296	175.540	1925.1	-	-	0.996	2.21	2.88				500.13		0.9973
CTb 231	39.300	175.539	1877.5	-	-	0.996	2.22	3.41	439	0.008	351	432.87	1.26	0.9978
CTb 232	39.300	175.539	1873.2	20	190	0.991	2.14	4.14				467.11		0.9979
CTb 233	39.300	175.539	1872.0	15	240	0.994	2.17*	2.83				465.89		0.9979
CTb 234	39.300	175.539	1873.4	-	-	0.996	2.15	3.16				467.11		0.9979
LC 254	39.272	175.605	1827.1	-	-	0.997	2.01	5.42	506	0.010	506	462.22	1.18	0.9981
LC 255	39.272	175.605	1826.6	-	-	0.997	2.07	6.43				461.00		0.9981
LC 256	39.272	175.605	1825.6	-	-	0.996	2.08	6.04				452.44		0.9980
LC 257	39.272	175.605	1824.7	16	330	0.996	2.05	3.68				462.22		0.9981
WG 325	39.256	175.555	2079.1	21	357	0.991	2.25	4.03	329	0.008	264	536.81	2.45	0.9966
WG 326	39.256	175.555	2066.7	-	-	0.995	2.30	3.15				520.91		0.9965
DC 327	39.235	175.551	1600.4	-	-	0.999	2.22	3.52	401	0.008	321	379.07	0.67	0.9987
DC 329	39.234	175.551	1591.8	-	-	0.999	2.37	4.34				380.29		0.9987
DC 330	39.234	175.551	1590.3	-	-	0.999	2.21	3.39				377.85		0.9987

Density measures were obtained with the hydrostatic method. Density values marked with * were calculated by averaging densities of other samples from the same site. P_{nuc}, Closure age, He_{nuc}, and P_4 values are considered equal for all samples of the same flow.

https://doi.org/10.5194/egusphere-2024-163
Preprint. Discussion started: 23 January 2024

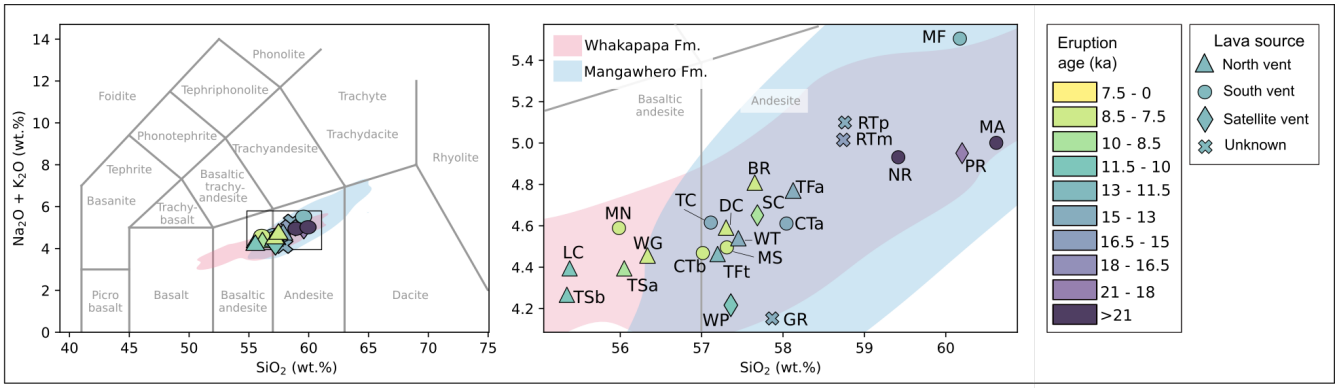

Figure A1. TAS classification diagram of the sampled lava flows (Le Maitre, 2002). Coloured areas represent geochemical ranges of Whakapapa and Mangawhero lavas.

https://doi.org/10.5194/egusphere-2024-163
Preprint. Discussion started: 23 January 2024

Author contributions.

PD carried out field sampling, mineral separation, He isotopes measurements, data processing and interpretation, and manuscript writing. SE assisted with sampling, data processing and manuscript revision. BK did the project supervision, obtained resources and reviewed the manuscript. PB helped with methodology, data analysis and paper revision. AN reviewed and edited the manuscript. GL helped with resources and data interpretation. DT assisted with data interpretation. JC helped with paper revision. CC helped with data interpretation. SB assisted with mineral separation. GF, LZ and BT helped with He isotopes measurements.

Competing interests.

We declare that none of the authors has competing interests.

Acknowledgements. We would like to acknowledge Ngāti Rangi, Uenuku and Ngāti Tūwharetoa Iwi, *tangata whenua* and guardians of Ruapehu. We are grateful to the Resilience to Nature Challenges (RNC) program, the Australian Institute of Nuclear Science and Engineering (AINSE), Mason Trust, The Royal Society of New Zealand, and The Tongariro Natural History Society for providing funds; the New Zealand's Department of Conservation for sampling permission; Amy Dreyer, Gilles Seropian and Alexander Marshall for assistance in the field; Hollei Gabrielsen for Māori subjects advise and aid with permit process; and Chris Grimshaw for help with laboratory procedures.

https://doi.org/10.5194/egusphere-2024-163
Preprint. Discussion started: 23 January 2024

References

Alcalá-Reygosa, J., Arce, J. L., Schimmelpfennig, I., Salinas, E. M., Rodríguez, M. C., Léanni, L., Aumaître, G., Bourlès, D., and Keddadouche, K.: Revisiting the age of the Jumento volcano, Chichinautzin Volcanic Field (Central Mexico), using in situ-produced cosmogenic 10Be, Journal of Volcanology and Geothermal Research, 366, 112–119, https://doi.org/10.1016/j.jvolgeores.2018.10.005, 2018.

Anderson, S. W., Krinsley, D. H., and Fink, J. H.: Criteria for recognition of constructional silicic lava flow surfaces, Earth Surface Processes and Landforms, 19, 531–541, https://doi.org/https://doi.org/10.1002/esp.3290190606, 1994.

Balco, G., Stone, J. O., Lifton, N. A., and Dunai, T. J.: A complete and easily accessible means of calculating surface exposure ages or erosion rates from 10Be and 26Al measurements, Quaternary Geochronology, 3, 174–195, https://doi.org/10.1016/j.quageo.2007.12.001, 2008.

Barrell, D. J.: Quaternary Glaciers of New Zealand, in: Developments in Quaternary Sciences, chap. 75, pp. 1047–1064, Elsevier, 15 edn., https://doi.org/https://doi.org/10.1016/B978-0-444-53447-7.00075-1, 2011.

Barrell, D. J. A., Almond, P. C., Vandergoes, M. J., Lowe, D. J., and Newnham, R. M.: A composite pollen-based stratotype for inter-regional evaluation of climatic events in New Zealand over the past 30,000 years (NZ-INTIMATE project), Quaternary Science Reviews, 74, 4–20, https://doi.org/10.1016/j.quascirev.2013.04.002, 2013.

Blard, P.-H.: Cosmogenic 3He in terrestrial rocks: A review, Chemical Geology, 586, 120 543, https://doi.org/10.1016/j.chemgeo.2021.120543, 2021.

Blard, P.-H. and Farley, K. A.: The influence of radiogenic 4He on cosmogenic 3He determinations in volcanic olivine and pyroxene, Earth and Planetary Science Letters, 276, 20–29, https://doi.org/10.1016/j.epsl.2008.09.003, 2008.

Blard, P.-H., Braucher, R., Lavé, J., and Bourlès, D.: Cosmogenic 10 Be production rate calibrated against 3 He in the high Tropical Andes (3800 – 4900 m , 20 – 22 ∘ S), Earth and Planetary Science Letters, 382, 140–149, https://doi.org/10.1016/j.epsl.2013.09.010, 2013.

Blard, P.-H., Balco, G., Burnard, P. G., Farley, K. A., Fenton, C. R., Friedrich, R., Jull, A. J., Niedermann, S., Pik, R., Schaefer, J. M., Scott, E. M., Shuster, D. L., Stuart, F. M., Stute, M., Tibari, B., Winckler, G., and Zimmermann, L.: An inter-laboratory comparison of cosmogenic 3He and radiogenic 4He in the CRONUS-P pyroxene standard, Quaternary Geochronology, 26, 11–19, https://doi.org/10.1016/j.quageo.2014.08.004, 2015.

Bromley, G. R., Winckler, G., Schaefer, J. M., Kaplan, M. R., Licht, K. J., and Hall, B. L.: Pyroxene separation by HF leaching and its impact on helium surface-exposure dating, Quaternary Geochronology, 23, 1–8, https://doi.org/10.1016/j.quageo.2014.04.003, 2014.

Calvert, A. T., Fierstein, J., and Hildreth, W.: Eruptive history of Middle Sister, Oregon Cascades, USA-Product of a late Pleistocene eruptive episode, Geosphere, 14, 2118–2139, https://doi.org/10.1130/GES01638.1, 2018.

Clay, P. L., Busemann, H., Sherlock, S. C., Barry, T. L., Kelley, S. P., and McGarvie, D. W.: 40Ar/39Ar ages and residual volatile contents in degassed subaerial and subglacial glassy volcanic rocks from Iceland, Chemical Geology, 403, 99–110, https://doi.org/10.1016/j.chemgeo.2015.02.041, 2015.

Coble, M. A., Grove, M., and Calvert, A. T.: Calibration of Nu-Instruments Noblesse multicollector mass spectrometers for argon isotopic measurements using a newly developed reference gas, Chemical Geology, 290, 75–87, https://doi.org/10.1016/j.chemgeo.2011.09.003, 2011.

Cole, J. W. and Lewis, K. B.: Evolution of the Taupo-Hikurangi subduction system, Tectonophysics, 72, 1–21, https://doi.org/10.1016/0040-1951(81)90084-6, 1981.

Conway, C. E.: Studies on the Glaciovolcanic and Magmatic Evolution of Ruapehu Volcano , New Zealand, Phd thesis, Victoria University of Wellington, https://researcharchive.vuw.ac.nz/handle/10063/5152, 2016.

https://doi.org/10.5194/egusphere-2024-163
Preprint. Discussion started: 23 January 2024

Conway, C. E., Townsend, D. B., Leonard, G. S., Wilson, C. J., Calvert, A. T., and Gamble, J. A.: Lava-ice interaction on a large composite volcano: a case study from Ruapehu, New Zealand, Bulletin of Volcanology, 77, https://doi.org/10.1007/s00445-015-0906-2, 2015.

Conway, C. E., Leonard, G. S., Townsend, D. B., Calvert, A. T., Wilson, C. J., Gamble, J. A., Eaves, S. R., Pure, L. R., Leonard, G. S., Townsend, D. B., Wilson, C. J., Calvert, A. T., Cole, R. P., Conway, C. E., Gamble, J. A., and Smith, T. B.: A high-resolution 40Ar/39Ar lava chronology and edifice construction history for Ruapehu volcano, New Zealand, Journal of Volcanology and Geothermal Research, 327, 152–179, https://doi.org/10.1016/j.jvolgeores.2016.07.006, 2016.

Donoghue, S. L.: Late quaternary volcanic stratigraphy of the southeastern sector of the Mount Ruapehu ring plain New Zealand, Ph.D. thesis, Massey University, https://mro.massey.ac.nz/items/516a0d80-eda3-4a7e-a495-2e13fcb7821c, 1991.

Donoghue, S. L. and Neall, V. E.: Late Quaternary constructional history of the southeastern Ruapehu ring plain, New Zealand, New Zealand Journal of Geology and Geophysics, 44, 439–466, https://doi.org/10.1080/00288306.2001.9514949, 2001.

Donoghue, S. L., Neall, V. E., and Palmer, A. S.: Stratigraphy and chronology of late quaternary andesitic tephra deposits, tongariro volcanic centre, new zealand, Journal of the Royal Society of New Zealand, 25, 115–206, https://doi.org/10.1080/03014223.1995.9517487, 1995.

Donoghue, S. L., Stewart, R. B., Neall, V. E., Lecointre, J., Price, R., Palmer, A. S., McClelland, E., and Hobson, K.: The Tau-rewa Eruptive Episode: Evidence for climactic eruptions at Ruapehu volcano, New Zealand, Bulletin of Volcanology, 61, 223–240, https://doi.org/https://doi.org/10.1007/s004450050273, 1999.

Donoghue, S. L., Vallance, J. W., Smith, I. E., and Stewart, R. B.: Using geochemistry as a tool for correlating proximal andesitic tephra : case studies from Mt Rainier (USA) and MT Ruapehu (New Zealand), Journal of Quaternary Science, 22, 395–410, https://doi.org/10.1002/jqs, 2007.

Dunai, T. J.: Cosmogenic Nuclides. Pinciples, Concepts and Application in the Earth Surface Sciences, Cambridge University Press, 2010.

Eaves, S. R. and Brook, M. S.: Glaciers and glaciation of North Island, New Zealand, New Zealand Journal of Geology and Geophysics, 64, 1–20, https://doi.org/10.1080/00288306.2020.1811354, 2021.

Eaves, S. R., Winckler, G., Schaefer, J. J. M., Vandergoes, M. J., Alloway, B. V., Mackintosh, A. N., Townsend, D. B., Ryan, M. T., and Li, X.: A test of the cosmogenic 3He production rate in the south-west Pacific (39°S), Journal of Quaternary Science, 30, 79–87, https://doi.org/10.1002/jqs.2760, 2015.

Eaves, S. R., Mackintosh, A. N., Anderson, B. M., Doughty, A. M., Townsend, D. B., Conway, C. E., Winckler, G., Schaefer, J. M., Leonard, G. S., and Calvert, A. T.: The Last Glacial Maximum in the central North Island, New Zealand: Palaeoclimate inferences from glacier modelling, Climate of the Past, 12, 943–960, https://doi.org/10.5194/cp-12-943-2016, 2016a.

Eaves, S. R., Mackintosh, A. N., Winckler, G., Schaefer, J. M., Alloway, B. V., and Townsend, D. B.: A cosmogenic 3He chronology of late Quaternary glacier fluctuations in North Island, New Zealand (39°S), Quaternary Science Reviews, 132, 40–56, https://doi.org/10.1016/j.quascirev.2015.11.004, 2016b.

Eaves, S. R., Winckler, G., Mackintosh, A. N., Schaefer, J. M., Townsend, D. B., Doughty, A. M., Jones, R. S., and Leonard, G. S.: Late-glacial and Holocene glacier fluctuations in North Island, New Zealand, Quaternary Science Reviews, 223, 105 914, https://doi.org/10.1016/j.quascirev.2019.105914, 2019.

Espanon, V. R., Honda, M., and Chivas, A. R.: Cosmogenic 3He and 21Ne surface exposure dating of young basalts from Southern Mendoza, Argentina, Quaternary Geochronology, 19, 76–86, https://doi.org/10.1016/j.quageo.2013.09.002, 2014.

Fleck, R. J., Hagstrum, J. T., Calvert, A. T., Evarts, R. C., and Conrey, R. M.: Ar / 39 Ar geochronology, paleomagnetism, and evolution of the Boring volcanic field , Oregon and Washington , USA, Geosphere, 10, 1283–1314, https://doi.org/10.1130/GES00985.1, 2014.

https://doi.org/10.5194/egusphere-2024-163
Preprint. Discussion started: 23 January 2024

Foeken, J. P., Day, S., and Stuart, F. M.: Cosmogenic 3He exposure dating of the Quaternary basalts from Fogo, Cape Verdes: Implications for rift zone and magmatic reorganisation, Quaternary Geochronology, 4, 37–49, https://doi.org/10.1016/j.quageo.2008.07.002, 2009.

Gamble, J. A., Price, R. C., Smith, I. E., McIntosh, W. C., and Dunbar, N. W.: 40Ar/39Ar geochronology of magmatic activity, magma flux and hazards at Ruapehu volcano, Taupo Volcanic Zone, New Zealand, Journal of Volcanology and Geothermal Research, 120, 271–287, https://doi.org/10.1016/S0377-0273(02)00407-9, 2003.

Gosse, J. J. C., Phillips, F. M., and Philips, F.: Terrestrial in situ cosmogenic nuclides: Theory and application, Quaternary Science Reviews, 20, 1475–1560, https://doi.org/10.1016/S0277-3791(00)00171-2, 2001.

Greve, A., Turner, G. M., Conway, C. E., Townsend, D. B., Gamble, J. A., and Leonard, G. S.: Palaeomagnetic refinement of the eruption ages of Holocene lava flows, and implications for the eruptive history of the Tongariro Volcanic Centre, New Zealand, Geophysical Journal International, 207, 702–718, https://doi.org/10.1093/gji/ggw296, 2016.

Hackett, W. R.: Geology and petrology of Ruapehu volcano and related vents, Phd thesis, Victoria University of Wellington, http://researcharchive.vuw.ac.nz/handle/10063/743, 1985.

Harpel, C. J., Kyle, P. R., Esser, R. P., McIntosh, W. C., and Caldwell, D. A.: 40Ar/39Ar dating of the eruptive history of Mount Erebus, Antarctica: Summit flows, tephra, and caldera collapse, Bulletin of Volcanology, 66, 687–702, https://doi.org/10.1007/s00445-004-0349-7, 2004.

Harris, A. J. L.: Basaltic Lava Flow Hazard, in: Volcanic Hazards, Risks and Disasters, edited by Shroder, J. F. and Papale, P., chap. Chapter 2, pp. 17–46, Elsevier, https://doi.org/10.1016/C2011-0-07012-6, 2015.

Houghton, B. F., Wilson, C. J., McWilliams, M. O., Lanphere, M. A., Weaver, S. D., Briggs, R. M., and Pringle, M. S.: Chronology and dynamics of a large silicic magmatic system: central Taupo Volcanic Zone, New Zealand, Geology, 23, 13–16, https://doi.org/10.1130/0091-7613(1995)023<0013:CADOAL>2.3.CO;2, 1995.

Jenkins, S. F., Day, S. J., Faria, B. V., and Fonseca, J. F.: Damage from lava flows: insights from the 2014–2015 eruption of Fogo, Cape Verde, Journal of Applied Volcanology, 6, https://doi.org/10.1186/s13617-017-0057-6, 2017.

Kurz, M. D.: Cosmogenic helium in a terrestrial igneous rock, Nature, 320, 435–439, https://doi.org/10.1038/320435a0, 1986.

Kurz, M. D., Colodner, D., Trull, T. W., Moore, R. B., and O'Brien, K.: Cosmic ray exposure dating with in situ produced cosmogenic 3He: results from young Hawaiian lava flows, Earth and Planetary Science Letters, 97, 177–189, https://doi.org/10.1016/0012-821X(90)90107-9, 1990.

Lal, D.: An important source of 4He (and 3He) in diamonds, Earth and Planetary Science Letters, 96, 1–7, https://doi.org/10.1016/0012-821X(89)90118-0, 1989.

Lal, D.: Cosmic ray labeling of erosion surfaces: in situ nuclide production rates and erosion models, Earth and Planetary Science Letters, 104, 424–439, https://doi.org/https://doi.org/10.1016/0012-821X(91)90220-C, 1991.

Le Maitre, R. W.: Igneous Rocks: A Classification and Glossary of Terms, Recommendations of the International Union of Geological Sciences, Subcomission of the Systematics of Igneous Rocks, Cambridge University Press, 2002.

Leonard, G. S., Cole, R. P. R., Christenson, B. W., Conway, C. E., Cronin, S. J., Gamble, J. A., Hurst, T., Kennedy, B. M., Miller, C. A., Procter, J. N., Pure, L. R., Townsend, D. B., White, J. D., and Wilson, C. J.: Ruapehu and Tongariro stratovolcanoes: a review of current understanding, New Zealand Journal of Geology and Geophysics, 64, 389–420, https://doi.org/10.1080/00288306.2021.1909080, 2021.

Leya, I., Lange, H. J., Neumann, S., Wieler, R., and Michel, R.: The production of cosmogenic nuclides in stony meteoroids by galactic cosmic-ray particles, Meteoritics and Planetary Science, 35, 259–286, https://doi.org/10.1111/j.1945-5100.2001.tb01845.x, 2000.

https://doi.org/10.5194/egusphere-2024-163
Preprint. Discussion started: 23 January 2024

Licciardi, J. M., Kurz, M. D., and Curtice, J. M.: Cosmogenic 3He production rates from Holocene lava flows in Iceland, Earth and Planetary Science Letters, 246, 251–264, https://doi.org/10.1016/j.epsl.2006.03.016, 2006.

Lifton, N.: Implications of two Holocene time-dependent geomagnetic models for cosmogenic nuclide production rate scaling, Earth and Planetary Science Letters, 433, 257–268, https://doi.org/10.1016/j.epsl.2015.11.006, 2016.

Lifton, N., Sato, T., and Dunai, T. J.: Scaling in situ cosmogenic nuclide production rates using analytical approximations to atmospheric cosmic-ray fluxes, Earth and Planetary Science Letters, 386, 149–160, https://doi.org/10.1016/j.epsl.2013.10.052, 2014.

Martin, L. C., Blard, P.-H., Balco, G., Lavé, J., Delunel, R., Lifton, N., and Laurent, V.: The CREp program and the ICE-D production rate calibration database: A fully parameterizable and updated online tool to compute cosmic-ray exposure ages, Quaternary Geochronology, 38, 25–49, https://doi.org/10.1016/j.quageo.2016.11.006, 2017.

Matsuda, J., Matsumoto, T., Sumino, H., Nagao, K., Yamamoto, J., Miura, Y., Kaneoka, I., Takahata, N., and Sano, Y.: The 3He/4He ratio of new internal He Standard of Japan (HESJ), Geochemical Journal, 36, 191–195, https://doi.org/10.2343/geochemj.36.191, 2002.

Mc Arthur, J. L. and Shepherd, M. J.: Late Quaternary glaciation of Mt. Ruapehu, North Island, New Zealand, Journal of the Royal Society of New Zealand, 20, 287–296, https://doi.org/10.1080/03036758.1990.10416823, 1990.

Morimoto, N., Fabries, J., Ferguson, A., Ginzburg, I., Ross, M., Seifert, F., Zussman, J., Aoki, K., and Gottardi, G.: Nomenclature of pyroxenes Subcommittee on Pyroxenes Commission on New Minerals and Mineral Names International Mineralogical Association, American Mineralogist, 73, 1123–1133, 1988.

Muscheler, R., Beer, J., Kubik, P. W., and Synal, H. A.: Geomagnetic field intensity during the last 60,000 years based on 10Be and 36Cl from the Summit ice cores and 14C, Quaternary Science Reviews, 24, 1849–1860, https://doi.org/10.1016/j.quascirev.2005.01.012, 2005.

Niedermann, S.: Cosmic-ray-produced noble gases in terrestrial rocks: Dating tools for surface processes, Reviews in Mineralogy and Geochemistry, 47, https://doi.org/10.2138/rmg.2002.47.16, 2002.

Nishiizumi, K.: Cosmic ray production rates of 10Be and 26Al in quartz from glacially polished rocks, Journal of Geophysical Research, 94, https://doi.org/10.1029/jb094ib12p17907, 1989.

Pardo, N.: Andesitic Plinian Eruptions at Mt. Ruapehu (New Zealand): From Lithofacies to Eruption Dynamics, Phd thesis, Massey University, https://mro.massey.ac.nz/items/c2f61b33-2579-410f-b493-eeab08691375, 2012.

Pardo, N., Cronin, S., Palmer, A., Procter, J., and Smith, I.: Andesitic Plinian eruptions at Mt. Ruapehu: Quantifying the uppermost limits of eruptive parameters, Bulletin of Volcanology, 74, 1161–1185, https://doi.org/10.1007/s00445-012-0588-y, 2012.

Parmelee, D. E., Kyle, P. R., Kurz, M. D., Marrero, S. M., and Phillips, F. M.: A new Holocene eruptive history of Erebus volcano, Antarctica using cosmogenic 3He and 36Cl exposure ages, Quaternary Geochronology, 30, 114–131, https://doi.org/10.1016/j.quageo.2015.09.001, 2015.

Patterson, D. B., Honda, M., and McDougall, I.: Noble gases in mafic phenocrysts and xenoliths from New Zealand, Geochimica et Cosmochimica Acta, 58, 4411–4427, https://doi.org/10.1016/0016-7037(94)90344-1, 1994.

Preece, K., Mark, D. F., Barclay, J., Cohen, B. E., Chamberlain, K. J., Jowitt, C., Vye-Brown, C., Brown, R. J., and Hamilton, S.: Bridging the gap: 40Ar/39Ar dating of volcanic eruptions from the 'Age of Discovery', Geology, 46, 1035–1038, https://doi.org/10.1130/G45415.1, 2018.

Price, R. C., Gamble, J. A., Smith, I. E., Maas, R., Waight, T., Stewart, R. B., and Woodhead, J.: The anatomy of an andesite volcano: A time-stratigraphic study of andesite petrogenesis and crustal evolution at Ruapehu Volcano, New Zealand, Journal of Petrology, 53, 2139–2189, https://doi.org/10.1093/petrology/egs050, 2012.

https://doi.org/10.5194/egusphere-2024-163
Preprint. Discussion started: 23 January 2024

Pure, L. R., Leonard, G. S., Townsend, D. B., Wilson, C. J., Calvert, A. T., Cole, R. P., Conway, C. E., Gamble, J. A., and Smith, T. B.: A high resolution 40Ar/39Ar lava chronology and edifice construction history for Tongariro volcano, New Zealand, Journal of Volcanology and Geothermal Research, 403, 106 993, https://doi.org/10.1016/j.jvolgeores.2020.106993, 2020.

Ramos, F. C., Heizler, M. T., Buettner, J. E., Gill, J. B., Wei, H. Q., Dimond, C. A., and Scott, S. R.: U-series and 40Ar/39Ar ages of Holocene volcanic rocks at Changbaishan volcano, China, Geology, 44, 511–514, https://doi.org/10.1130/G37837.1, 2016.

Rhodes, E.: The Draining of an Andesitic Valley-Confined Lava Flow, Mt Ruapehu, Honours thesis, University of Canterbury, 2012.

Schaefer, J. M., Winckler, G., Blard, P.-H., Balco, G., Shuster, D. L., Friedrich, R., Jull, A. J. T., Wieler, R., and Schluechter, C.: Performance of CRONUS-P - A pyroxene reference material for helium isotope analysis, Quaternary Geochronology, 31, 237–239, https://doi.org/10.1016/j.quageo.2014.07.006, 2016.

Schimmelpfennig, I., Williams, A., Pik, R., Burnard, P., Niedermann, S., Finkel, R., Schneider, B., and Benedetti, L.: Inter-comparison of cosmogenic in-situ 3He, 21Ne and 36Cl at low latitude along an altitude transect on the SE slope of Kilimanjaro volcano (3°S, Tanzania), Quaternary Geochronology, 6, 425–436, https://doi.org/10.1016/j.quageo.2011.05.002, 2011.

Sherrod, D. R., Hagstrum, J. T., Mcgeehin, J. P., Champion, D. E., and Trusdell, F. A.: Distribution , 14 C chronology , and paleomagnetism of latest Pleistocene and Holocene lava flows at Haleakala Island of Maui , Hawai ‘ i : A revision of lava flow hazard zones, Journal of Geophysical Research, 111, https://doi.org/10.1029/2005JB003876, 2006.

Shuster, D. L., Farley, K. A., Sisterson, J. M., and Burnett, D. S.: Quantifying the diffusion kinetics and spatial distributions of radiogenic 4He in minerals containing proton-induced 3He, Earth and Planetary Science Letters, 217, 19–32, https://doi.org/10.1016/S0012-821X(03)00594-6, 2004.

Stipp, J.: The Geochronology and Petrogenesis of the Cenozoic Volcanics of the North Island, New Zealand, Phd thesis, Australian National University, 1968.

Stone, J. O.: Air pressure and cosmogenic isotope production, Journal of Geophysical Research,, 105, 753–759, https://doi.org/https://doi.org/10.1029/2000JB900181, 2000.

Tanaka, H., Kawamura, K., Nagao, K., and Houghton, B. F.: K-Ar ages and paleosecular variation of direction and intensity from quaternary lava sequences in the Ruapehu Volcano, New Zealand, Earth, Planets and Space, 49, 587–599, https://doi.org/https://doi.org/10.5636/jgg.49.587, 1997.

Topping, W. W.: Some aspects of quaternary history of Tongariro Volcanic Centre, Phd thesis, Victoria University of Wellington, 1974.

Topping, W. W. and Kohn, B. P.: Rhyolitic tephra marker beds in the Tongariro area, North Island, New Zealand, New Zealand Journal of Geology and Geophysics, 16, 375–395, https://doi.org/10.1080/00288306.1973.10431367, 1973.

Townsend, D., Leonard, G., Conway, C., Eaves, S., and Wilson, C.: Geology of the Tongariro National Park Area, GNS Science, pp. 1 sheet + 109 pp, 2017.

Trusdell, F. A.: Lava flow hazards and risk assessment on Mauna Loa Volcano, Hawaii, Geophysical Monograph Series, 92, 327–336, https://doi.org/10.1029/GM092p0327, 1995.

Tsang, S. and Lindsay, J.: Lava flow crises in inhabited areas part I: Lessons learned and research gaps related to effusive, basaltic eruptions, Journal of Applied Volcanology, 9, 1–26, https://doi.org/10.1186/s13617-020-00096-y, 2020.

Turner, G. M. and Corkill, R. M.: NZPSV11k.2023 and NZPSV1k.2023: Holocene palaeomagnetic secular variation master records for New Zealand, Physics of the Earth and Planetary Interiors, 344, 107 093, https://doi.org/10.1016/j.pepi.2023.107093, 2023.

Turner, G. M., Howarth, J. D., de Gelder, G. I., and Fitzsimons, S. J.: A new high-resolution record of Holocene geomagnetic secular variation from New Zealand, Earth and Planetary Science Letters, 430, 296–307, https://doi.org/10.1016/j.epsl.2015.08.021, 2015.

https://doi.org/10.5194/egusphere-2024-163
Preprint. Discussion started: 23 January 2024

Uppala, S. M., Kållberg, P. W., Simmons, A. J., Andrae, U., da Costa Bechtold, V., Fiorino, M., Gibson, J. K., Haseler, J., Hernandez, A., Kelly, G. A., Li, X., Onogi, K., Saarinen, S., Sokka, N., Allan, R. P., Andersson, E., Arpe, K., Balmaseda, M. A., Beljaars, A. C., van de Berg, L., Bidlot, J., Bormann, N., Caires, S., Chevallier, F., Dethof, A., Dragosavac, M., Fisher, M., Fuentes, M., Hagemann, S., Hólm, E., Hoskins, B. J., Isaksen, L., Janssen, P. A., Jenne, R., McNally, A. P., Mahfouf, J. F., Morcrette, J. J., Rayner, N. A., Saunders, R. W., Simon, P., Sterl, A., Trenberth, K. E., Untch, A., Vasiljevic, D., Viterbo, P., and Woollen, J.: The ERA-40 re-analysis, Quarterly Journal of the Royal Meteorological Society, 131, 2961–3012, https://doi.org/10.1256/qj.04.176, 2005.

Wijbrans, J., Schneider, B., Kuiper, K., Calvari, S., Branca, S., De Beni, E., Norini, G., Corsaro, R. A., and Miraglia, L.: 40Ar/39Ar geochronology of Holocene basalts; examples from Stromboli, Italy, Quaternary Geochronology, 6, 223–232, https://doi.org/10.1016/j.quageo.2010.10.003, 2011.

Wilson, C. J., Gravley, D. M., Leonard, G. S., and Rowland, J. V.: Volcanism in the central Taupo Volcanic Zone, New Zealand: tempo, styles and controls, in: Studies in Volcanology: The Legacy of George Walker, edited by Thordarson, T., pp. 225–247, Special Publications of IAVCEI 2, 2009.

Wilson, G., Wilson, T. M., Deligne, N. I., and Cole, J. W.: Volcanic hazard impacts to critical infrastructure: A review, Journal of Volcanology and Geothermal Research, 286, 148–182, https://doi.org/10.1016/j.jvolgeores.2014.08.030, 2014.

Wright, H. M., Vazquez, J. A., Champion, D. E., Calvert, A. T., Mangan, M. T., Stelten, M., Cooper, K. M., Herzig, C., and Jr, A. S.: Episodic Holocene eruption of the Salton Buttes rhyolites, California, from paleomagnetic, U-Th, and Ar/Ar dating Heather, Geochemistry, Geophysics, Geosystems, 16, 1198–1210, https://doi.org/10.1002/2015GC005714.Received, 2015.

Zimmermann, L., Avice, G., Blard, P.-H., Marty, B., Füri, E., and Burnard, P. G.: A new all-metal induction furnace for noble gas extraction, Chemical Geology, 480, 86–92, https://doi.org/10.1016/j.chemgeo.2017.09.018, 2018.